

See discussions, stats, and author profiles for this publication at: <https://www.researchgate.net/publication/361679412>

Flood susceptibility mapping of Northeast coastal districts of Tamil Nadu India using Multi-source Geospatial data and Machine Learning techniques

Article in *Geocarto International* · June 2022

DOI: 10.1080/10106049.2022.2096702

CITATIONS

43

READS

1,131

2 authors:



Saravanan Subbarayan

National Institute of Technology Tiruchirappalli

120 PUBLICATIONS 1,896 CITATIONS

[SEE PROFILE](#)



Abijith Devanantham

National Institute of Technology Tiruchirappalli

35 PUBLICATIONS 721 CITATIONS

[SEE PROFILE](#)



Flood susceptibility mapping of Northeast coastal districts of Tamil Nadu India using Multi-source Geospatial data and Machine Learning techniques

Subbarayan Saravanan & Devanantham Abijith

To cite this article: Subbarayan Saravanan & Devanantham Abijith (2022): Flood susceptibility mapping of Northeast coastal districts of Tamil Nadu India using Multi-source Geospatial data and Machine Learning techniques, *Geocarto International*, DOI: [10.1080/10106049.2022.2096702](https://doi.org/10.1080/10106049.2022.2096702)

To link to this article: <https://doi.org/10.1080/10106049.2022.2096702>



Published online: 10 Jul 2022.



Submit your article to this journal 



Article views: 63



View related articles 



View Crossmark data 



Flood susceptibility mapping of Northeast coastal districts of Tamil Nadu India using Multi-source Geospatial data and Machine Learning techniques

Subbarayan Saravanan  and Devanantham Abijith 

Department of Civil Engineering, National Institute of Technology, Tiruchirappalli, Tamil Nadu, India

ABSTRACT

Flooding is one of the most challenging and important natural disasters to predict, it is becoming more frequent and more intense. The study area is badly damaged by devastating flood in 2015. We assessed the flood susceptibility to northern coastal area of Tamil Nadu using various machine learning algorithms such as Gradient Boosting Machine (GBM), XGBoost (XGB), Rotation Forest (RTF), Support Vector Machine (SVM), and Naive Bayes (NB). Google Earth Engine (GEE) is used to demarcate flooded areas using Sentinel-1 and other multi-source geospatial data to generate influential factors. Recursive Feature Elimination (RFE) removes weak factors in this study. The flood susceptibility resultant map is classified into five classes: very low, low, moderate, high, and very high. The GBM algorithm attained high classification accuracy with an area under the curve (AUC) value of 92%. The study area is urbanized and vulnerable identifying flood inundation useful for effective planning and implementation.

ARTICLE HISTORY

Received 8 March 2022
Accepted 27 June 2022

KEYWORDS

Flood susceptibility;
machine learning; GEE;
GBM; XGBoost; RTF;
SVM; NB

1. Introduction

Climate change has impacted in past decades, leading to increase extreme precipitation and significant flooding (Singh and Saravanan 2020; Abraham and Kundapura 2022; Jose et al. 2022). Though water is a valuable renewable resource, flooding is a massive environmental hazard that may cause socioeconomic losses and property damage (Minh et al. 2019). Catastrophic flooding is mainly triggered due to massive short-duration, high-intensity rainfall, snowmelt, cloud burst and is also caused due to other poor geo-environmental conditions (Chakrabortty et al. 2021; Saha et al. 2021). Flooding is a complex and site-dependent phenomenon that has piqued scientist's interest in investigating, analysing, and comprehending its causes, owing primarily to large-scale environmental degradation caused by urban growth, riverside flood plain encroachment, urbanisation, deforestation, and other factors (Hong et al. 2018b; Kalantari et al. 2019). Water is responsible for approximately 74% of these natural disasters (Rahman et al. 2021c). Floods and storms are responsible for 69% of the financial losses, exposing over three billion people and killing 166,000 people worldwide (Amarasinghe et al. 2020). A hazard becomes a disaster

when it causes severe physical and social property loss in a flood-prone area (Parthasarathy and Deka 2019).

For several decades, the India Meteorological Department (IMD) has been observing monsoon trends to understand the El Niño Southern Oscillation (ENSO), which is a natural process caused by sea surface temperature (SST) oscillations induced by trade wind strengthening and weakening. ENSO is divided into El Niño, the warmer (positive phase), and La Niña, the colder (negative phase). Each phase could occur every two to seven years (Ju and Slingo 1995; Sagarika et al. 2016; Tamaddun et al. 2019). ENSO influence on flood hazards is critical in predicting the potential impacts of occurrences and possible preparation for the socioeconomic impacts of changes (Ward et al. 2014). Cyclones occur across several coasts of Andhra Pradesh, Orissa, Tamil Nadu, and West Bengal and are sometimes accompanied by significant rainfall, resulting in floods (Saravanan et al. 2018).

The Indian subcontinent is one of the world's most disaster-prone places, with about 85 percent of its geographical area subject to single or multiple hazards (Bilham and Bali 2014; Saravanan et al. 2019b; Jacinth Jennifer and Saravanan 2020; Parthasarathy et al. 2022). Coastal, flash, urban, fluvial, and pluvial flooding occur in India. Floods in India account for more than 40% of all-natural catastrophic mortality (Rahman et al. 2021b). Centre for Research on the Epidemiology of Disasters (CRED) reports that India lost almost 2% of its GDP. Due to its physical, topographical, and meteorological factors, it is one of the ten most disaster-prone countries (Parida 2020). Between 1980 and 2017, India witnessed 235 floods, killing 126,286 people, and affecting 1.93 billion people. Flood-related economic loss accounted for more than \$58.7 billion. Some notable floods in India are Uttarakhand (2013), Kashmir (2014), Chennai (2015), Patna (2019), and Kerala in 2018 and 2019 (Parthasarathy et al. 2021). In November and early December 2015, Southeast India, particularly Tamil Nadu and the adjacent union territory of Pondicherry, witnessed severe rainfall activity due to three heavy to catastrophic rainfall storms, resulting in disastrous floods across Tamil Nadu (Boyaj et al. 2018; Lal et al. 2020; George et al. 2022). Due to severe rains connected with depressions and cyclonic storms, Chennai is devastated by riverine floods and drainage system failures in 1943, 1976, 1985, 1996, 1998, 2005, and 2010 (Guhathakurta et al. 2011; Chakraborty 2016).

Remote sensing is a reliable and consistent method of providing synoptic coverage over a vast region at high efficiency. The area and extent of permanent water bodies and flood inundation may be determined more easily from remote sensing data. Although satellite-imaging platforms acquire permanent water body extent, microwave sensors can map floodwaters in small to medium-sized catchments under any meteorological conditions using Synthetic Aperture Radar (SAR) imaging sensor (Jacinth Jennifer et al. 2020). Furthermore, multi-date images provide investigators with an extra tool for tracking the change or reconstructing the development of previous flood-affected scenarios (Schumann and Moller 2015).

Google Earth Engine (GEE) is a cloud-based platform for efficiently processing satellite data for research, education, and non-profit purposes. GEE simplifies the specification of different modes of operation for integrating input data, efficiently creating composite data, cloud-free, and multi-temporal datasets (Abijith and Saravanan 2021; Kulithalai Shiyam Sundar and Deka 2021). In this study, we used Flood Mapping Algorithm (FMA) using GEE to calculate flood inundation extents (Rahman et al. 2021a). The European Space Agency's (ESA) Sentinel-1 C-band SAR mission provides free SAR data (Jacinth Jennifer et al. 2022). Previous studies have indicated that SAR datasets are best suited for mapping and monitoring flood extent.

There are five major approaches for generating flood susceptibility maps including multi-criteria decision analysis (MCDA) methods, statistical methods, physically-based models, deep learning methods and machine learning methods. Some MCDA models such as AHP, analytic network process MIF, Technique for order preference by similarity to an ideal solution (TOPSIS), and VlseKriterijumska optimizacija I Kompromisno Resenjeand VIKOR methods depend on expert opinion thus the results are somewhat partial and uncertain (Chowdary et al. 2013; Vojtek et al. 2021; Saleh et al. 2022). Bivariate statistical analysis (BSA) and multivariate statistical analysis (MSA) are two types of statistical methods. In the statistical model Frequency ratio (Sarkar and Mondal 2019), Dempster-Shafer-based evidential belief function (Tehrany and Kumar 2018), the weight of evidence (Hong et al. 2018c) are the bivariate statistical analysis, and Logistic regression (Al-Juaidi et al. 2018) is multivariate statistical analysis are mostly used where they rely on predicted variables which are based on linear assumptions, whereas flooding is typically non-linear. Physically based models (PBM) such as One-dimensional and two-dimensional models (Ghimire et al. 2020) are commonly used. PBM requires substantial computational resources, which is a drawback. While machine learning (ML) methods are better at solving non-linear problems, their accuracy is sensitive to the quality of the sample points (Tehrany et al. 2013). Whereas Deep learning (DL) models rely a vast amount of data to effectively execute and analyse, while the ML algorithms are executed in a precise way based on established rules (Costache et al. 2020; Ahmed et al. 2021; Pham et al. 2021). In recent years, ML models have identified themselves as major competitors to traditional statistical models in susceptibility assessment. ML approaches in flood susceptibility assessment are increasing due to their ability to extract associations efficiently using past occurrences and topography. Researchers are interested in susceptibility mapping because ML methods are useful in determining the dynamic relationships between the environmental variables (Mohammadi et al. 2020). The functional relationship between the significant variables could be an important factor in predicting flood and other environmental disasters. ML models have been explored because they can detect flood-prone locations based on historical events without necessarily understanding the physical processes behind them (Wang et al. 2015; Bera et al. 2022). Guyon et al. (2002) established the Recursive Feature Elimination (RFE) algorithm to improve feature selection while utilizing SVMs. They become relatively sub-optimal when it comes to eliminating several features at once, which is essential to produce a narrow feature subset. The invention of the neural network model in the 1980s sparked the commencement of research. Following that, research expanded the notion to include additional models, such as Support Vector Machines (SVM), Decision Trees (DT), Artificial Neural Networks (ANN), Random Forest (RF), Logistic Regression (LR), Particle swarm optimization (Sachdeva et al. 2017), Logistic Model Trees (LMT), Reduced Error Pruning Trees (REPT), Naïve Bayes Trees (NBT), Alternating Decision Trees (ADT) (Khosravi et al. 2018), Adaptive neuro-fuzzy inference system (Vafakhah et al. 2020), Artificial Neural Networks (Falah et al. 2019), Reduced-error pruning trees (REPTree) with Bagging (Bag-REPTree) and Random subspace (RS-REPTree) (Chen et al. 2019), Back propagation artificial neural network (Mudashiru et al. 2021), Boosted regression trees (Abedi et al. 2021), Deep Belief Network (DBN) (Shahabi et al. 2021), GAM: generalized additive model (Band et al. 2020a), MARS: multivariate adaptive regression splines (Tien Bui et al. 2019a), MaxEnt: maximum entropy (Javidan et al. 2021), PSO: particle swarm optimization (Arabameri et al. 2022), RTF: rotation forest (Rodríguez et al. 2006), SIA: swarm intelligence algorithm (Tien Bui et al. 2019b), Kernel Logistic Regression (KLR), Radial Basis Function Classifier (RBFC), Multinomial Naïve Bayes (NBM), and Logistic Model

Tree (LMT) (Pham et al. 2020), NB: Naïve Bayes (Chen et al. 2020), AdaBoost: adaptive boosting (Pham et al. 2021) are referred to together as machine learning models. The application of these models is typically attributed to their inherent simplicity in both comprehension and implementation. Furthermore, prediction abilities are improved by optimization and ensemble approaches at a low cost in terms of time/memory/computation. Among the numerous approaches, machine learning has gotten a lot of attention from researchers and engineers.

The primary goal of this research is to incorporate multi-satellite products and GIS-based data into the methodology for determining flood susceptibility in the northern coastal regions of Tamil Nadu. Narasimhan et al. (2016) calculated the return period of the rainfall event using IMD's fine resolution gridded daily data and concluded that the 2015 extreme rainfall event is found to be rare with a return period close to 100 years in the observed record. Historically, this area has been highly vulnerable to natural disasters such as flooding, shoreline change, sea level rise, and tsunami. The study comprises nineteen flood geo-environmental causative parameters with five ML models (GBM, XGBoost, RTF, SVM, and NB) compared and there are no studies on flood susceptibility mapping using ML algorithms for the Tamil Nadu coastal regions. Indices such as accuracy and the receiver operating characteristic (ROC) curve are used to evaluate model performance in training and testing datasets. The predicted output is used for creating the final flood susceptibility map for the region. These maps may help in flood planning and mitigation purposes for the future flood affecting areas and would support local authorities in identifying sensitive regions for appropriate warning and alert can be issued by the responsible authority to do the evacuation and reallocation of people from the vulnerable zone.

2. Material and methods

2.1. Study area

The study area (Figure 1) is situated in the Southern part of India i.e. Northern coast of Tamil Nadu comprising five districts (Chennai, Tiruvallur, Kanchipuram, Villupuram, and Cuddalore) and a union territory (Pondicherry). It spreads along the Bay of Bengal with a coastal length of 264 km. The total region comprised by the study is 6447.12 km² and lies between 79° 30' to 80° 21'E longitude and 10° 55' to 13° 33'N latitude, including elevations ranging from mean sea level to 210 m. The climate has mostly been tropical semiarid, and its geographical location tends to make it one of the country's most vulnerable coastal states, particularly during tropical cyclones and storm surges (Saleem Khan et al. 2020). According to the IPCC (2022) report, there would have historically been an increase in temperature and rainfall throughout the southern states of India. There has also been a lot of variation in rainfall across the states over the last few decades. The occurrence of heavy rainfall events is expected to increase by one to five events per year. Hence for the 25-kilometer distance landward from its administrative boundary of TN northern coast, the flood susceptibility mapping has been carried out where the area is frequently subjected to adverse conditions for flood. During the North East monsoon (October–December), the average rainfall is around 950 mm, accounting for approximately 48% of the annual average rainfall and annual temperature of 24.3 to 32.9°. Coastal ecosystems found include mudflats, sand dunes and the Pichavaram mangrove forest, one of the world's largest mangrove forests. The rivers flow from west to east until they reach the Bay of Bengal. The Palar, Cauvery, and Pennar are the well-known rivers flowing in this region. The Cauvery River is the largest estuary in the region, apart from

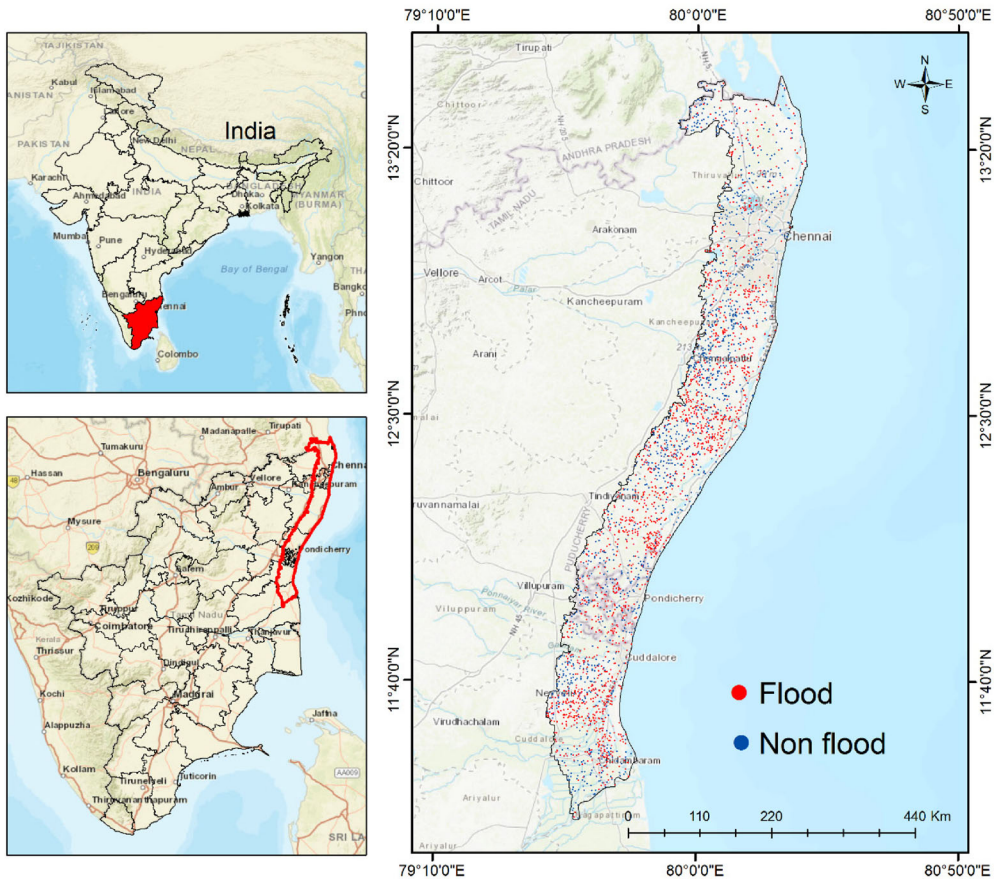


Figure 1. Study area location.

it smaller estuaries consist of Vellar, Pennar, and Adyar. The area is known to have two major and two minor ports, fishing harbors, coastal industries, nuclear and thermal power plants, refineries, and fertilizer plants (Saravanan et al. 2019a; Saranya and Saravanan 2021, 2022).

2.2. Flood causative factors

Identifying the conditioning variables from literature, previous flooding, and regional geo-environmental conditions is an essential step in determining the flood susceptibility. Based on the above-mentioned factors nineteen flood causative parameters such as slope, aspect, elevation, plan curvature, profile curvature, SPI, TWI, STI, TRI, rainfall, distance to road, distance to stream, distance to coast, LULC, soil, geology, geomorphology, wind, and NDVI are considered. The data are prepared from various sources and are shown in Table 1.

Topography is a significant land-surface feature that influences most characteristics of a catchment's surface and subsurface runoff. We require high-quality DEM data to assess how water interacts with the environment and to identify areas where floods are most likely to cause problems for people and property. The accuracy of water depth forecasts is

Table 1. Data sources.

Parameters	Data source	Source location	Resolution (m)
LULC, NDVI	Landsat 8 from GEE	https://code.earthengine.google.com/	30*30
Rainfall	Chirps from GEE	https://code.earthengine.google.com/	
DEM, TWI, SPI, TRI, STI, Slope, Profile and plan Curvature, Aspect, Wind	Shuttle Radar Topography Mission (SRTM) Land Processes Distributed Active Archive Center OpenStreetMap	https://lpdaac.usgs.gov/ https://www.openstreetmap.org	
Road Network, Stream Network			
Coast line	Shoreline	https://www.ngdc.noaa.gov/mgg/shorelines/	
Geology, Geomorphology,	Bhukosh	https://bhukosh.gsi.gov.in/Bhukosh/	
Soil	National Bureau of Soil Survey and Land Use Planning (NBSS and LUP)	https://www.nbsslup.in/	

related to the DEM's accuracy and spatial resolution (Sanyal and Lu 2004; Vaze et al. 2010; Wang et al. 2010). In this study, we used SRTM DEM (**Figure 2A**) which is 30 m resolution and open source provided by USGS. The research area is flat and low-lying and as a result, flooding is a regular occurrence throughout the region.

Regarding flood-related research, the slope is important because it governs surface water flow and has control over surface runoff. Slopes (**Figure 2B**) are determined by elevation contours that are directly related to flow velocity, lithology, structure, soil type, and drainage (Adiat et al. 2012; Zzaman et al. 2021). For estimating the direction of water flow from the cell to the neighboring cells, the elevation values of each cell are compared in GIS with the elevations of adjoining cells (Al-Juaidi et al. 2018). Aspect (**Figure 2C**) influences the flow direction for the flow of flooded water. Curvature is the rate at which the slope changes in a specific direction which is divided into three types: flat, convex, and concave. It is another influencing aspect of flood investigation (Lee et al. 2017; Tehrany et al. 2019). The profile curvature (**Figure 2D**) is also computed, that is the difference between convex and concave surfaces. Plan curvature (**Figure 2E**) is the curvature of an isoline formed by joining a horizontal plane and the land surface (Moore et al. 1991; Pouyan et al. 2021). The stream power index (SPI) (**Figure 2F**) measures the power of a stream's flow in terms of erosion and it is crucial for numerous processes in the fluvial environment (Jebur et al. 2014). The topographic wetness index (TWI) (**Figure 3A**) calculates the quantity of flow accumulation at every point in a drainage basin as well as the water's potential to go downslope under gravity (Das 2019). The Sediment Transport Index (STI) (**Figure 3B**) could provide significant information on the possibility of sediment movement in the stream network. It takes into account the influence of topography on erosion and characterizes erosion and deposition processes, as well as a flood conditioning factor that specifies the motions of waterborne sediments caused by water movement (Rahmati et al. 2019). The terrain ruggedness Index (TRI) (**Figure 3C**) computed as the mean difference between a center pixel and its surrounding cells in a DEM, represents soil saturation and the amount of water that may be retained (Lindsay et al. 2019).

When soil humidity is high and runoff is severe it has an indirect impact on the extent of flooding (Towfiqul Islam et al. 2021; Sachdeva and Kumar 2022) and the soil map is shown in (**Figure 3D**). The cumulative rainfall of the torrential rainfall period (November–December 2015) (**Figure 3E**) layer is created using data from Climate Hazards Group Infra-Red Precipitation with Station data (CHIRPS) and the rainfall map have five classes ranging from 564 to 990 mm. Rainfall floods are denoted as flooding

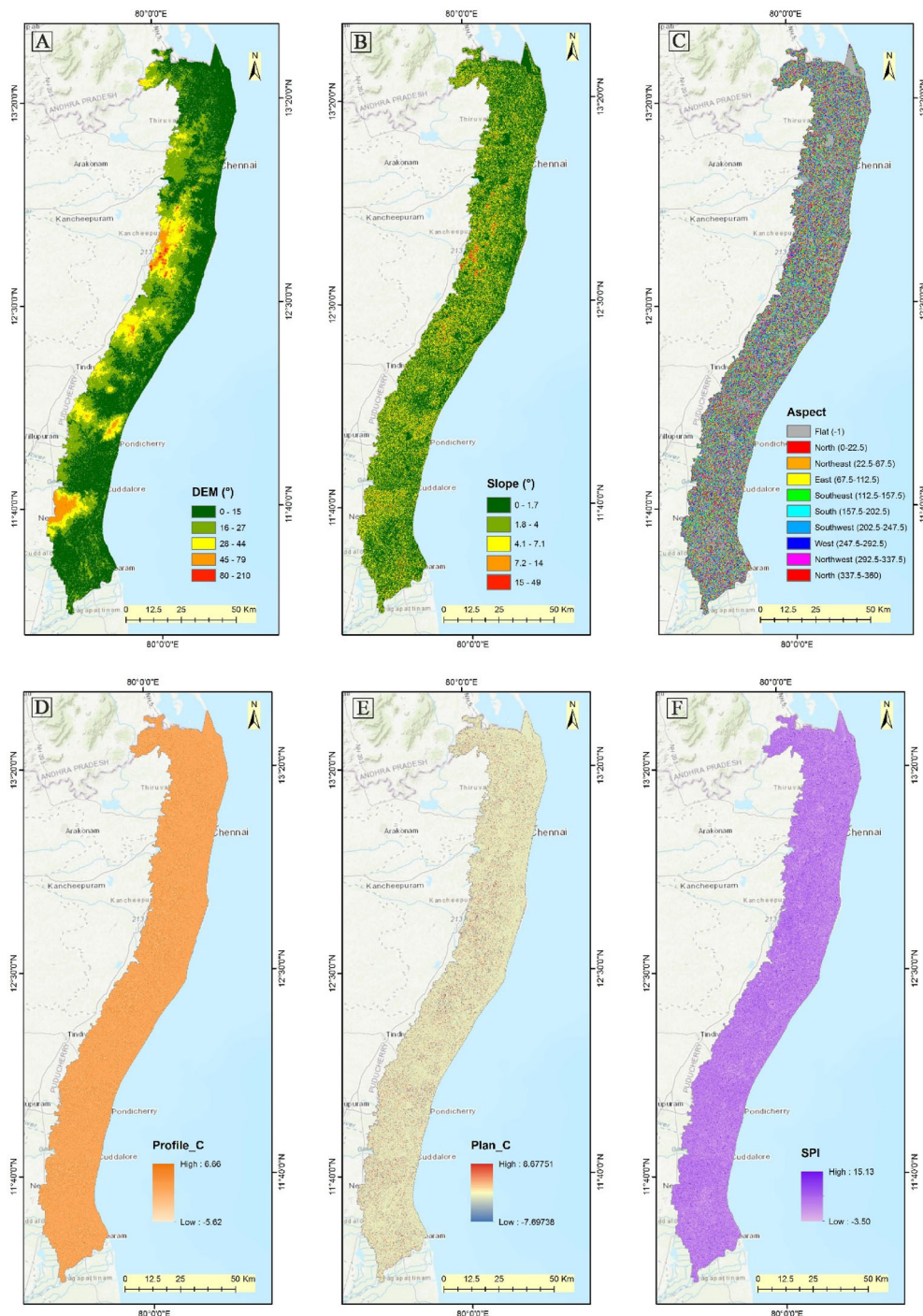


Figure 2. Causative factors used in this study: (A) DEM, (B) Slope, (C) Aspect, (D) Profile_C, (E) Plan_C, (F) SPI.

caused by rainfall directly in a short duration, including urban storm floods and surplus water in non-urban regions. Rainfall may occur with lesser intensity (about 10 mm/h) but for a longer duration, particularly if the ground surface is impermeable can cause flood

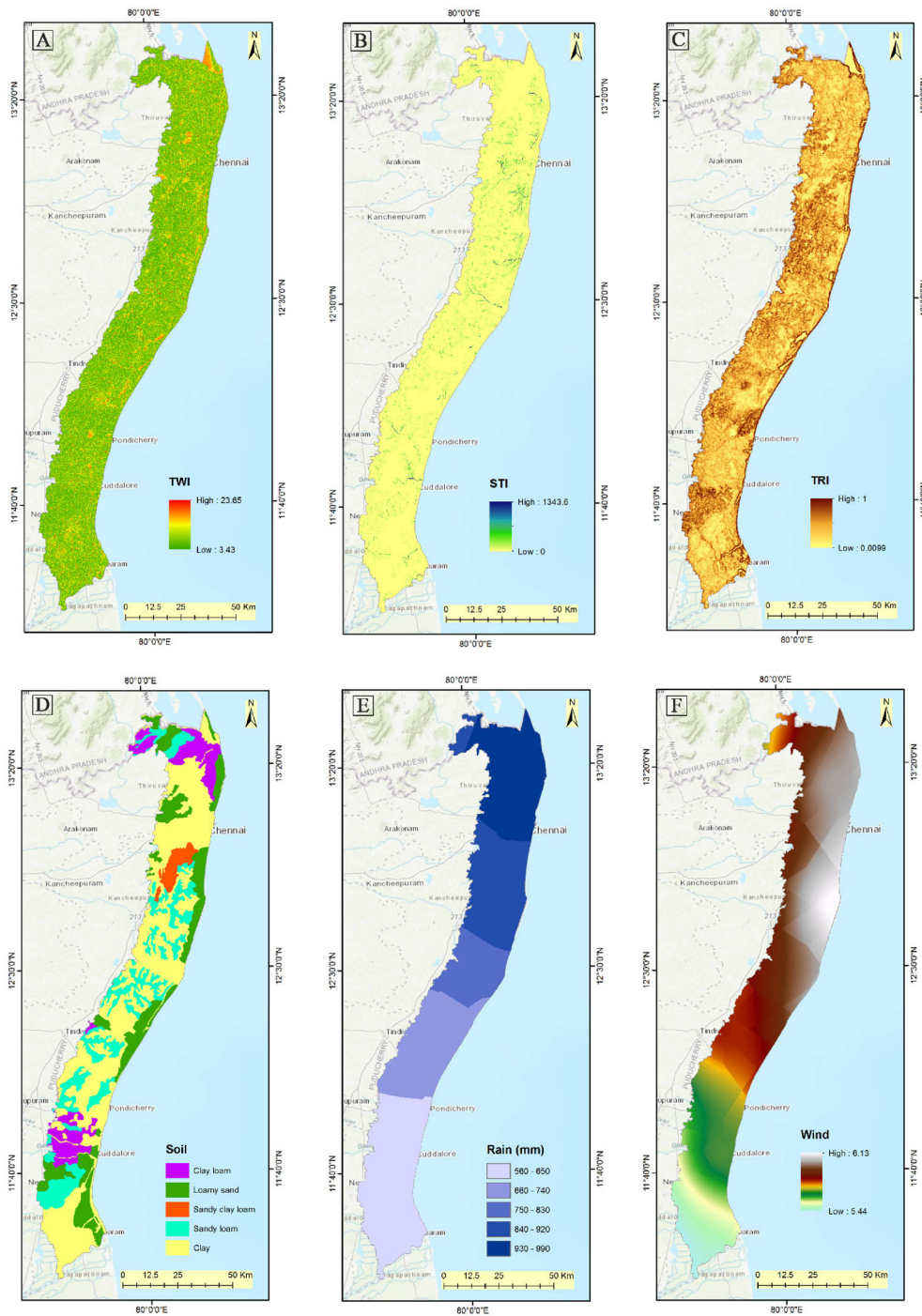


Figure 3. Causative factors used in this study: (A) TWI, (B) STI, (C) TRI, (D) Soil, (E) Rain, (F) Wind.

(Shen et al. 2019; Walczykiewicz and Skonieczna 2020). Wind (m/s) (Figure 3F) plays a stronger role in the generation of storm surge and tide levels, a connection exists between surge height and wind speed (Joyce 2017; Abijith et al. 2021).

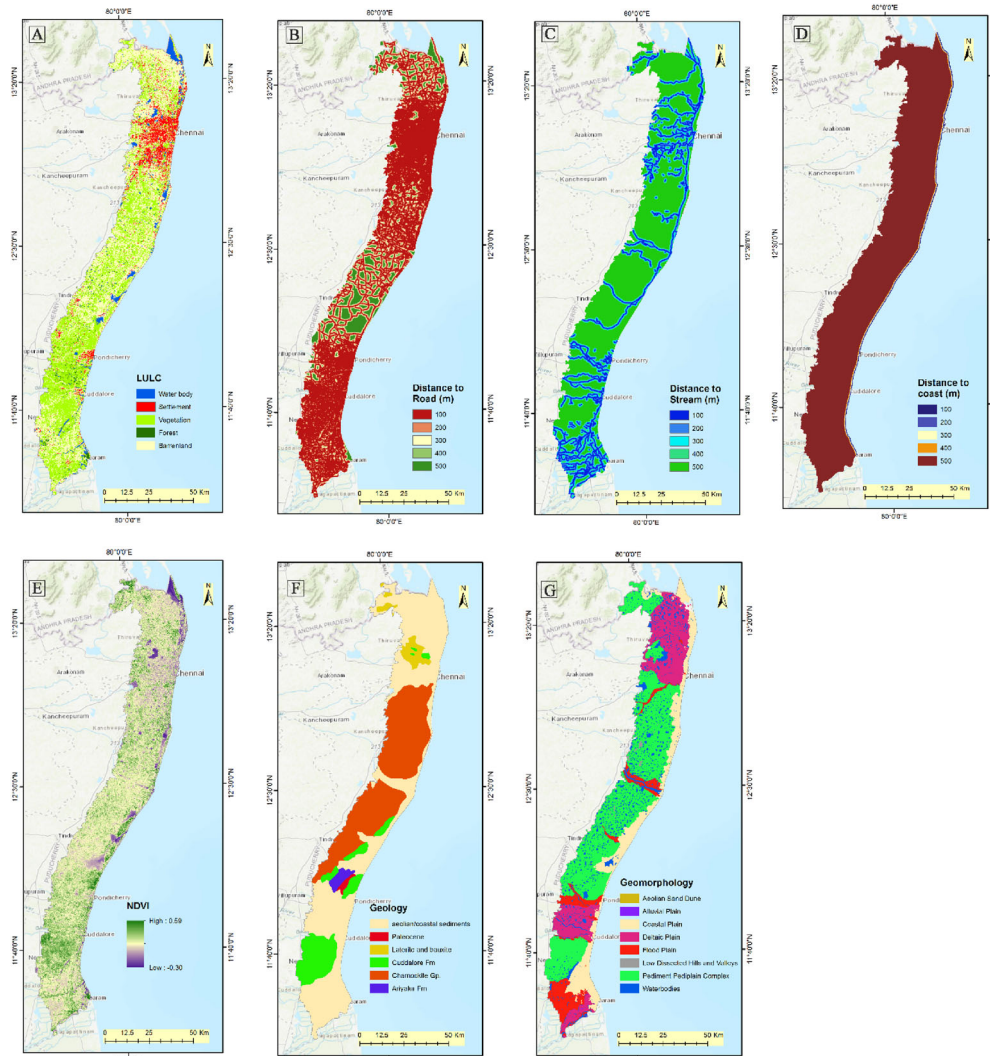


Figure 4. Causative factors used in this study: (A) LULC, (B) Distance to Road, (C) Distance to River, (D) Distance to Coast, (E) NDVI, (F) Geology, (G) Geomorphology.

The Landsat data is used to generate the LULC (Figure 4A), which is then processed in GEE using the Random Forest (RF) algorithm. GEE assists researchers in predicting the map patterns and quantity differences on the Earth's surface by analyzing data at a planetary scale (Kulithalai Shiyam Sundar and Deka 2021). In this study, Landsat 8 TOA reflectance has been used for LULC classification and is classified into five classes: settlement, waterbody, barren land, forest, and agriculture.

Road (Figure 4B), river (Figure 4C), and coast (Figure 4D) features are extracted from the OpenStreetMap which is an open-source map tool to download the vector layers. The coastline is obtained from the National Geophysical Data Center. The grading approach is carried out for the distance to road, rivers, and coast using the 'Euclidean' distance tool. Road development increases the proportion of impermeable surfaces, resulting in lower groundwater recharge and changes in topography, which cause flow accumulation and

excessive runoff (Swain et al. 2020). Flooding typically occurs along the river's bank, inundating low-lying flood plain areas. The distance from the river has a considerable influence on the severity of the flood. The distance from the coast is a critical hint in determining the flooded area. During the heavy rainfall and storm surge, the areas closest to the beaches are the most impacted by the flood (Gesch 2018; Samanta et al. 2018). The Normalized Difference Vegetation Index (NDVI) (Figure 4E) is a reliable index for evaluating vegetation cover and its impact on flooding. Geology (Figure 4F) and geomorphology (Figure 4G) such factor is closely connected to the permeability of the rocks. The infiltration of rainwater is less important for an impermeable rock, which enhances water stagnation and the addition of runoff surfaces, thereby increasing flood risks (Hammami et al. 2019).

2.3. Flood inventory map

The flood inventory map comprises 1500 flood-affected pixels locations. The inundated places are determined using (i) historical flood data from the reports, (ii) field surveys and (iii) SAR imagery. Sentinel-1 data is utilized in the GEE platform to map the flooded regions. The technique uses two Sentinel-1 imagery (i.e. before and after the flood) that is pre-processed to compute the backscatter coefficient in decibels after eliminating thermal noise, radiometric calibration, and terrain correction. The script computes the difference between the two imagery before applying a smoothing filter to reduce the influence of speckle noise. A threshold is applied to the smoothed image to detect the potentially flooded regions. The Sentinel-1 imagery acquired in September 2015 is used as a reference image for the before flood scenario, and November 14, 2015, is used for the after-flood scenario where the flood reached its peak in the region, thus the frequently flooded region is extracted, and converted into points. The non-flood points are derived from location information that are not flooded during the flooding event, and from the expert's knowledge.

The methodological flow chart shows (Figure 5) the overview of the overall work carried out, including the flood inventory map, generation of flood conditioning factors, evaluation of machine learning methods (GBM, XGBoost, RTF, SVM, NB using accuracy and ROC-AUC.

2.4. Recursive feature elimination (RFE)

RFE is a feature selection approach that fits a model and eliminates the weakest feature (or features) until the desired amount of features is attained. In this study, eight categorical (slope, aspect, elevation, plan curvature, profile curvature, SPI, TWI, STI, TRI, rainfall, wind, and NDVI) and eleven numerical data (distance to road, distance to stream, distance to coast, LULC, soil, geology, geomorphology) are present. Each class in the categorical data is separated into each layer to convert it into a numerical data, where the number of layers is equal to the sum of total number of classes in all the eight categorical data. In R program, Min-Max Normalization technique is carried out using Scale function. Features are prioritized using the model's coefficients or feature importance's attributes, and RFE aims to minimize dependencies and collinearity in the model by iteratively deleting a minimal number of features every iteration. This is used in the next phase to define the optimal feature selection, which is preferred as the optimal feature configuration from iteration, with the better workable approach in terms of higher Kappa. From the result (Figure 6), 17 parameters that are the important feature contributing to the flood are obtained, with the kappa value of 0.6364 and accuracy of 0.818 in the set of 100 iterations.

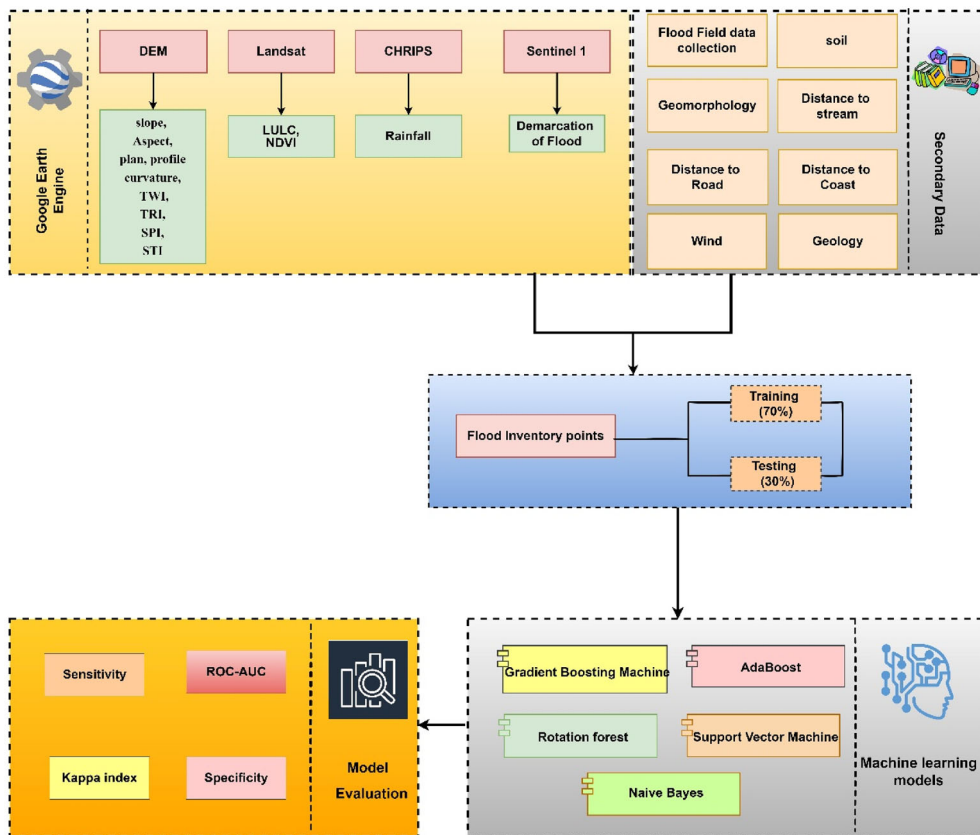


Figure 5. Process flowchart.

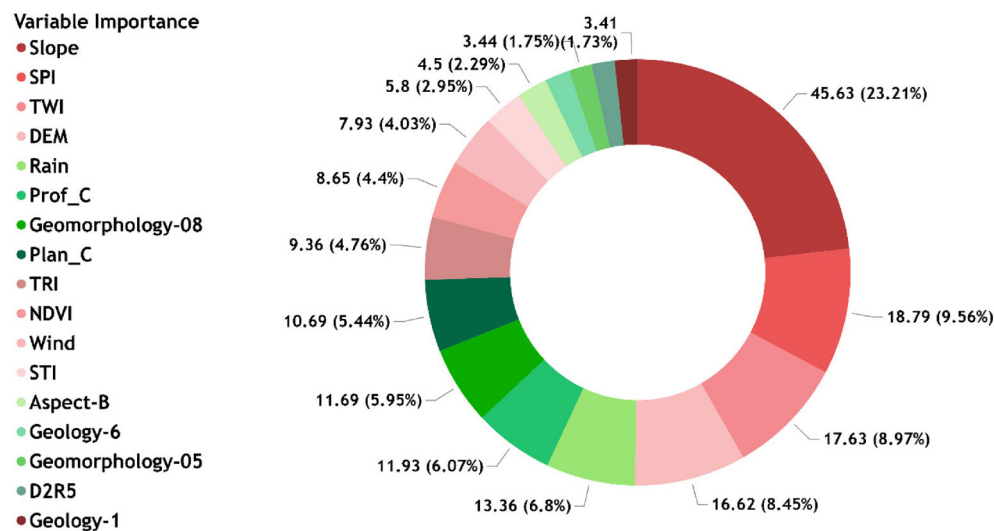


Figure 6. RFE feature importance.

2.5. Machine learning based flood susceptibility mapping

In this study, five machine learning models are used (GBM, XGBoost, RTF, SVM, NB) to assess the relationship between explanatory factors and flooding to generate flood hazard maps combining the best predictions of the preceding models. All of the causative factors are created in the GIS environment and the models are built using the Caret package in R studio.

2.5.1. Gradient boosting machine (GBM)

Friedman (2001) proposed the GBM algorithm, which is also an ensemble learning model, integrates multiple decision trees to generate an even more comprehensive tool that can be used for classification or regression. This method mainly builds new base learners that are supremely correlated with the negative gradient of the loss function associated with the entire ensemble. Rather than RF, each tree in GBM tries to fix the error of the previous tree (Akinci et al. 2021). To achieve this, the same residual errors determined as a result, the previous predicted trees are minimized, the next tree is acquired, and all these tasks are repeated till the prediction results are reliable or the maximum number of trees is attained (Ayyadevara 2018; Sahin 2020).

2.5.2. XGBoost

Chen and Guestrin (2016) proposed the XGBoost algorithm, which is currently the best and better decision tree algorithm. It prunes the tree as well as manages missing data (Abedi et al. 2021). It reduces a regularised objective function in conjunction with a weighting factor for model complexity. This operation in particular, uses parallel processes while training the model to ensure quick learning. Since there are so many parameters to train when modelling, data can be managed to learn in a dynamic way (Fan et al. 2018). An XGBoost algorithm creates the poor classification prediction model and then appraises its performance using a training dataset (Friedman 2001; Madhuri et al. 2021; Krishnaraj and Honnasiddaiah 2022).

2.5.3. Rotation forest (RTF)

Rotation forest (RTF) is a machine learning ensemble approach proposed by (Rodríguez et al. 2006). The focus of rotation forest is to increase member diversity as well as individual accuracy within an ensemble classifier (Naghibi et al. 2019). Training each base classifier on various subsamples considerably improves the difference between the base classifiers and helps in boosting prediction accuracy after integration. A classifier on the features that the matrix repetitively develops, as well as the outcome, is achieved by integrating the output of the various classifiers (Al-Abadi 2018; Fang et al. 2021).

2.5.4. Support vector machine (SVM)

SVM is a novel supervised learning approach applied to classification as well as regression which is built on the structural risk minimization concept, has been proven to be a reliable and efficient method for equation fitting, data analysis, hydrological forecasting, and other applications (Belousov et al. 2002; Byun and Lee 2002; Tehrany et al. 2015; Yan et al. 2018). The primary benefit of the SVM model is that it may minimize error testing and model complexity. The kernel function is the mathematical operation that is utilized to transform data. An ideal hyper-plane is employed in the SVM model to segregate the original input space. The kernel function is used for data transformations, such as

categorizing the data set as flood or non-flood, which are specified by 1 and 0, respectively (Samui 2008; Pradhan 2013; Tehrany et al. 2015).

2.5.5. Naive Bayes

To maximize posterior probability, Nave Bayes is a statistical classification technique used to determine the class used for classification based on the assumption that there is no dependency of both attributes (Hong et al. 2018a; Lee et al. 2020; He et al. 2021; Janizadeh et al. 2021). The Naive Bayes classifier implies that the impact of predictor cost (x) on a specific category (c) of predictor values is neutral (Janizadeh et al. 2021).

2.6. Accuracy assessment

The ROC curve is a graphical tool used to evaluate the model's performance. The y-axis represents sensitivity and the x-axis represents specificity. To predict the model's accuracy, a specific decision criterion can be extracted for each point on the ROC curve. The area under the ROC curve (AUC) is used to assess model performance quantitatively; the higher the value of AUC (in the case of an accurate model, AUC is close to 1), the better the model's performance (Pham and Prakash 2017; Band et al. 2020b). The sensitivity of a flooded cell is the probability that it is correctly classified. The false-negative rate is the sensitivity of a flooded cell. The probability that a non-flood cell is correctly classified is referred to as specificity. The false-positive rate is defined as specificity. The ROC which is an integral part of the ROC curve, is a statistical metric commonly used to assess the performance of flood models. Sensitivity (SS), specificity (SP), positive predictive (PP), and negative predictive (NP) are used in statistical indices. If the results of these indices are higher, therefore every ML model performed best, and vice versa.

$$SS = \frac{TP}{TP + FN} \quad (1)$$

$$SS = \frac{TN}{FP + TN} \quad (2)$$

$$PP = \frac{TP}{FP + TP} \quad (3)$$

$$NP = \frac{TN}{TN + FN} \quad (4)$$

where TP—true positive, TN—true negative, FP—false positive, and FN—false negative.

3. Results

3.1. Flood susceptibility map

Flood susceptibility maps are generated using GBM, XGboost, RTF, SVM, and NB models and presented in the following section. The prediction outputs for all five models use the natural break classification method to categorise the outputs into five classes, namely very low, low, moderate, high, and very high. Jenks optimization, also known as natural break classification, is a data categorization process used to evaluate the optimal value impact of various classes. This classification technique tries to reduce the average disparity between classes while increasing the disparity among the entire class. As a result, the process removes intraclass disparities while increasing group disparities. Areas with a higher

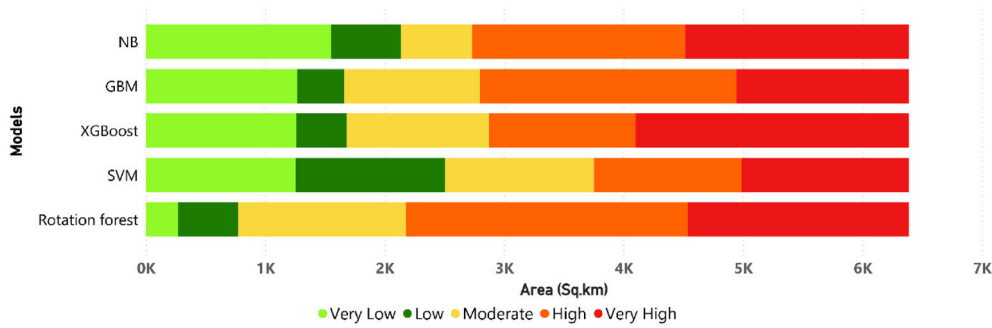


Figure 7. Change in area.

rating are more prone to floods, and vice versa. This is useful because it generates maps with accurate representations of data trends (Arabameri et al. 2020; Ahmadlou et al. 2021). Figure 7 shows the flooded areas in square kilometres for the different models. Figure 8 depicts the percentile of variables their importance versus models (as the DEM shows 100% due to the scaling it has not been included in the graph).

3.1.1. GBM

The model's variable importance as shown in Figure 8 represents that DEM (100%) has the higher importance in this model followed by TWI (5%), slope (3.76%), ge8-waterbody (3.026%), plan_C (2.482%), rain (1.576%), TRI (1.38%), whereas ge6-deltaic plain, NDVI, STI, g6-coastal sediments, ge2-pediment Pedi plain complex, ge5-coastal Plain, s1-loamy sand scores importance less than 1%. Unlike other models, GBM shows very less variable importance. Model accuracy for GBM is evaluated using ROC to select the optimal model using the largest value. The final values used for the model are n.trees = 100, interaction_depth = 2, shrinkage = 0.1 and n.minobsinnode = 10. n.minobsinnode is the one that separates each node until the terminal node gets up to one input (Figure 9A). The accuracy 0.92%, kappa 0.82%, sensitivity 0.98% and specificity 0.81% values for the testing dataset. Thus, the GBM susceptibility map is shown in Figure 10, which is divided into five zones based on its susceptibility. The results show that the least area of 391.73 sq. km falls into the low susceptibility zone, followed by the moderate zone of area 1136.54 sq. km, the very low susceptibility zone covers an area of 1269.14 sq. km, the very high zone comprises 1442.03 sq. km, and the large sector falls under the high susceptibility zone of area 2149.28 sq. km.

3.1.2. XGBoost

The flood susceptibility map for the XGBoost is shown in Figure 11, which is divided into five zones based on its susceptibility. The very least area of 419.44 sq. km falls under the low susceptibility zone, followed by the moderate zone of 1191.02 sq. km, high 1228.90 sq. km, and very low 1262.76. The majority of the area comprising 2286.59 sq. km falls under the very high susceptibility zone. From the models variable importance (Figure 8) DEM (100) has the highest importance in this model followed by TWI (13.39%), slope (18.93%), ge8-waterbody (5.06%), plan_C (10.89%), rain (18.52%), TRI (14%), NDVI (10.27%), whereas ge6-deltaic Plain, STI, g6-coastal sediments, ge2-pediment Pedi plain complex, ge5-coastal plain, s1-loamy sand are less 10%. In this model, the tuning parameter 'gamma' is held at a constant value of 0. Tuning parameter 'min_child_weight' is held constant at a value of 1 where 'min_child_weight' is used to control over-fitting and is the sample size below which the model cannot divide a node. Higher values prohibit a

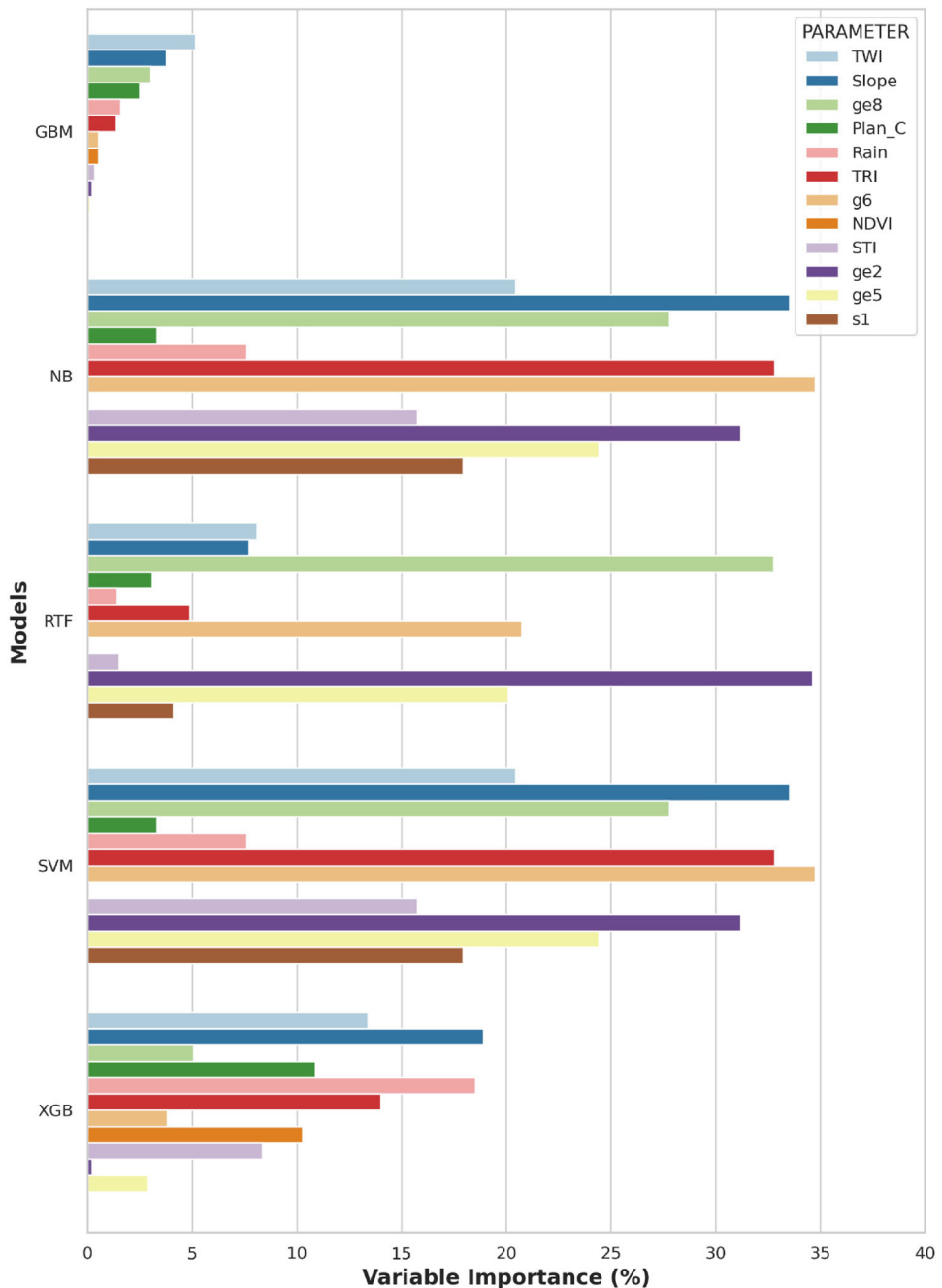


Figure 8. Model vs. variable importance in percent.

model from learning relations that are particularly unique to the sample used for a tree. The final values used for the model are nrounds = 50, max_depth = 1, eta = 0.4, gamma = 0, colsample_bytree = 0.8, min_child_weight = 1 and subsample = 0.625 ([Figure 9B](#)). The accuracy is 96%, kappa 92%, sensitivity 98%, and specificity 90% values for the testing dataset.

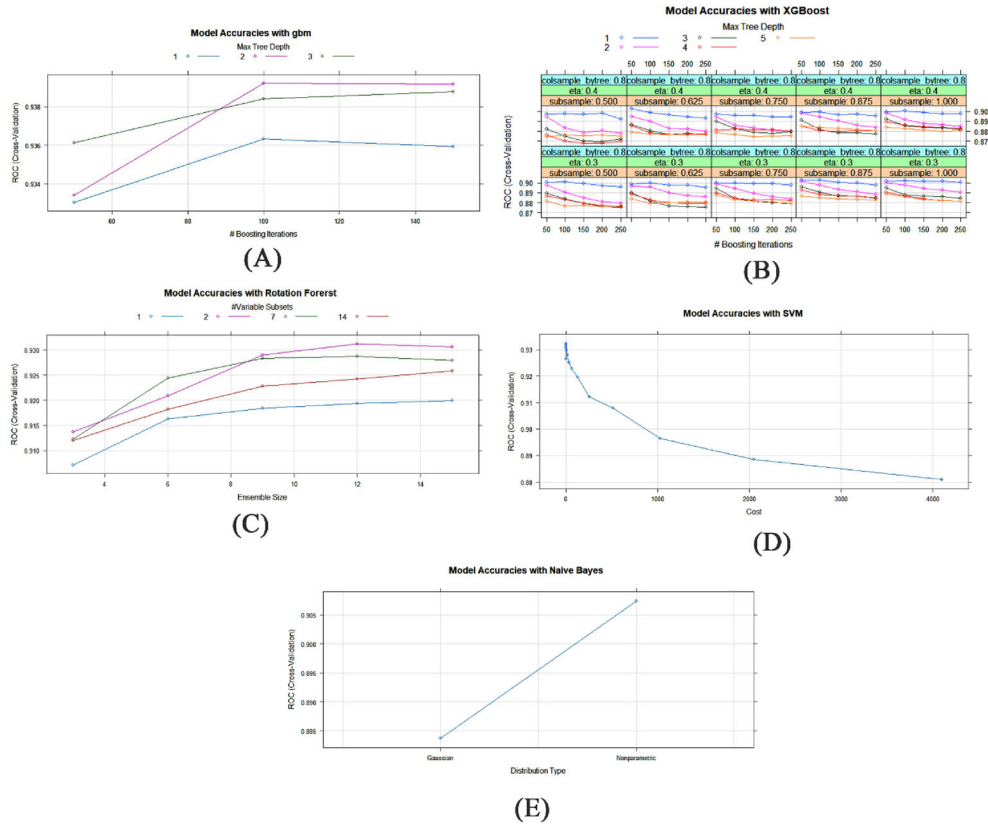


Figure 9. Model accuracy (A) GBM, (B) XGB, (C) RTF, (D) SVM, (E) NB.

3.1.3. Rotation forest

The flood susceptibility map for the RTF is shown in Figure 12, which is divided into five zones based on its susceptibility. The results show that the least area of 270.945 sq. km falls into the very low susceptibility zone, followed by the low susceptibility zone of area 503.402 sq. km, the moderate susceptibility zone covers around 1404.02 sq. km, the very high susceptibility zone of 1850.16 sq. km, and the majority area of about 2360.19 sq. km falls into the high susceptibility zone. From the variable importance (Figure 8) slope (100) has the highest importance in this model followed by TWI (8.10%), slope (7.71%), ge8-waterbody (32.76%), plan_C (3.08%), ge6-deltaic Plain (24.61%), g6-coastal sediments, ge2-pediment Pedi plain complex (34.62%), ge5-coastal plain (20.10%), whereas rain, TRI, STI, NDVI, and s1-Loamy sand has importance less than 5%. ROC is used to select the optimal model using the largest value. The final values used for the model are K=2 and L=12 where K denotes the number of factors randomly assigned to a single tree and L is the total number of trees in the forest (Figure 9C). The accuracy and kappa of the models are 91% and 80% respectively. The sensitivity and specificity score the value of 97% and 80%.

3.1.4. SVM

The flood susceptibility map for the SVM is shown in Figure 13, which is divided into five zones based on its susceptibility. Compared to other models, the areal extent seems to have minor variation as very low, low, medium, high, and very high zones depict the

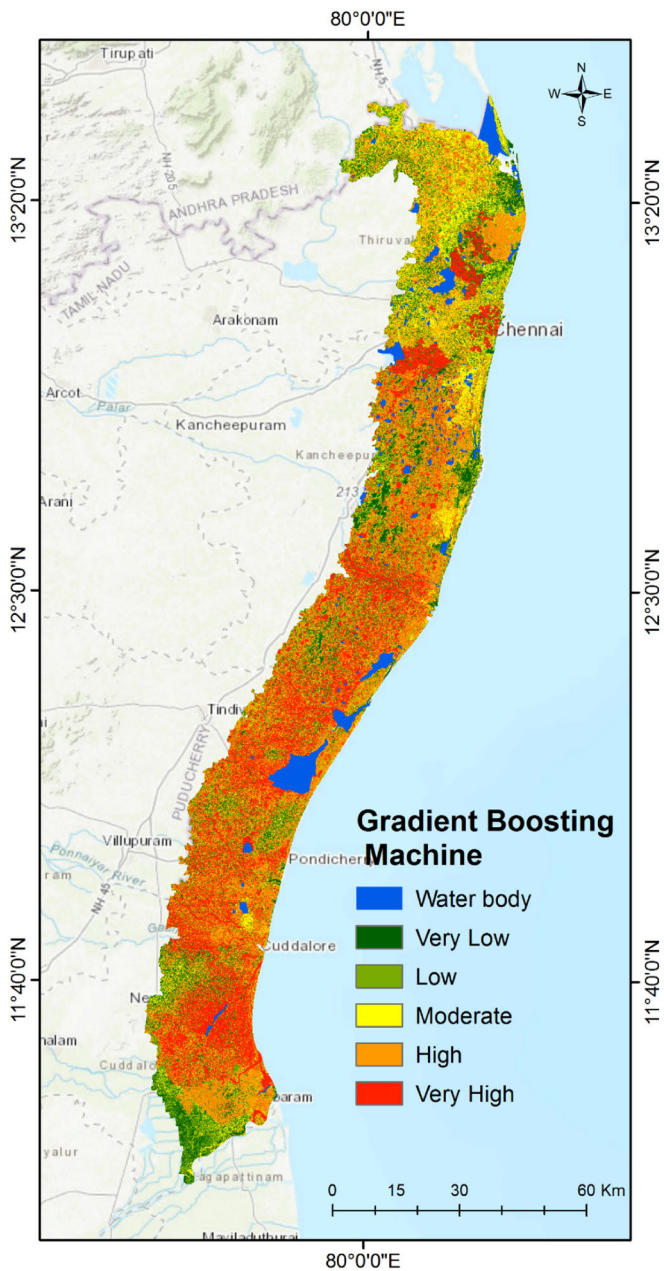


Figure 10. Flood susceptibility map-GBM model.

areal coverage of 1254.33 sq. km, 1250.67 sq. km, 1247.35 sq. km, 1237.84 sq. km, and 1398.52 sq. km respectively. From the variable importance (Figure 8). DEM (100) has the highest importance in this model followed by TWI (20.44%), slope (33.53%), ge8-waterbody (27.79%), TRI (32.81%), ge6-deltaic Plain (25.60%), g6-coastal sediments (43.89%), ge2-pediment Pedi plain complex (31.20%), ge5-coastal plain (24.42%), STI (15.77%), s1-loamy sand (17.93%), whereas NDVI, plan_C and rain, are less than 10%. Tuning parameter sigma and C are held at a constant value of 0.05829778 and 1 respectively

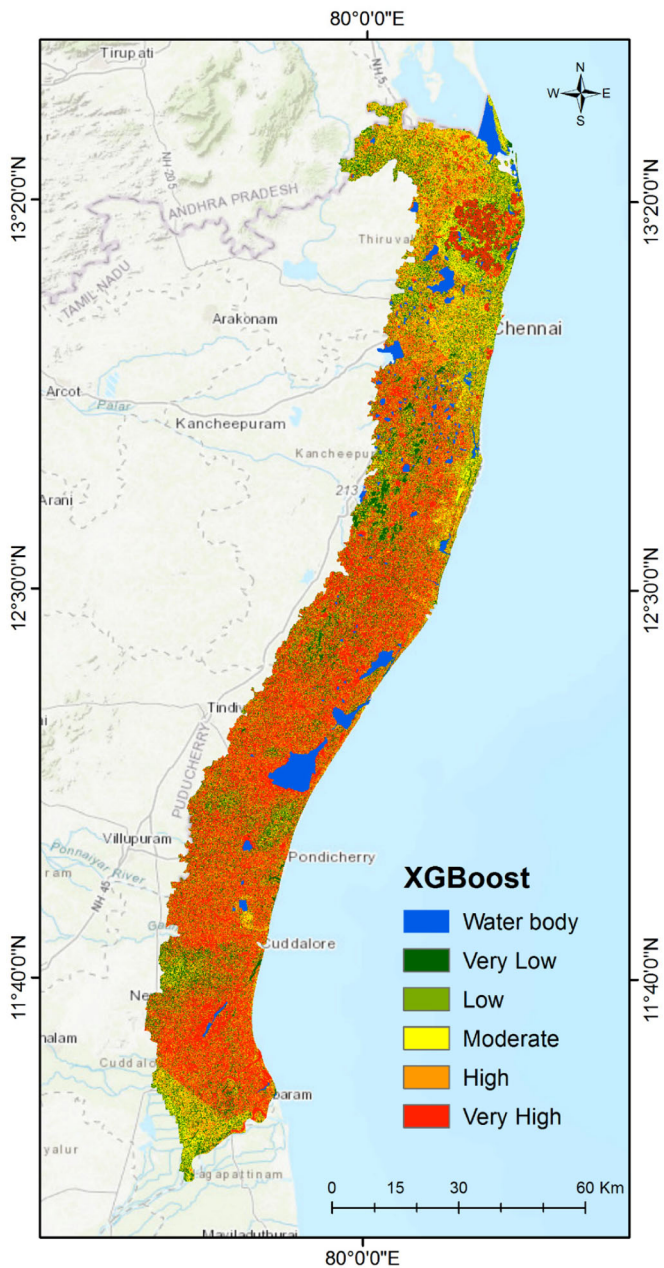


Figure 11. Flood susceptibility map-XGBoost model.

(Figure 9D). Sigma parameter regulates the amount of nonlinearity added into the model. The decision boundary is significantly non-linear if the sigma value is very low. If the sigma value is high the decision boundary tends to be linear. ROC is used to select the optimal model using the largest value. The model and kappa for the SVM are 91% and 82% respectively, and the sensitivity and specificity scores a value of 97% and 81% respectively for the testing dataset.

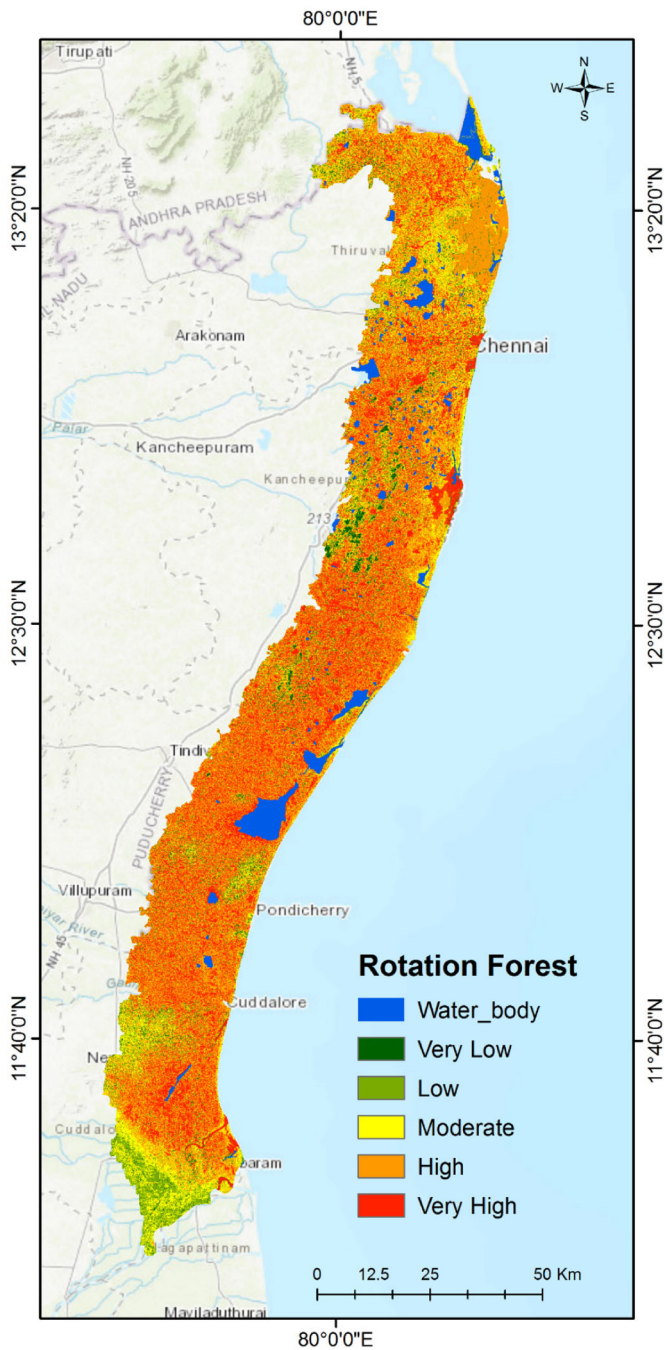


Figure 12. Flood susceptibility map-Rotation forest model.

3.1.5. Naïve Bayes

The flood susceptibility map for the NB is shown in Figure 14, which is divided into five zones based on its susceptibility. The results show that the least area of 583.54 sq. km falls into the low susceptibility zone, followed by the moderate zone of area 596.475 sq. km, the very low susceptibility zone covers around 1552.08 sq. km, the high susceptibility zone

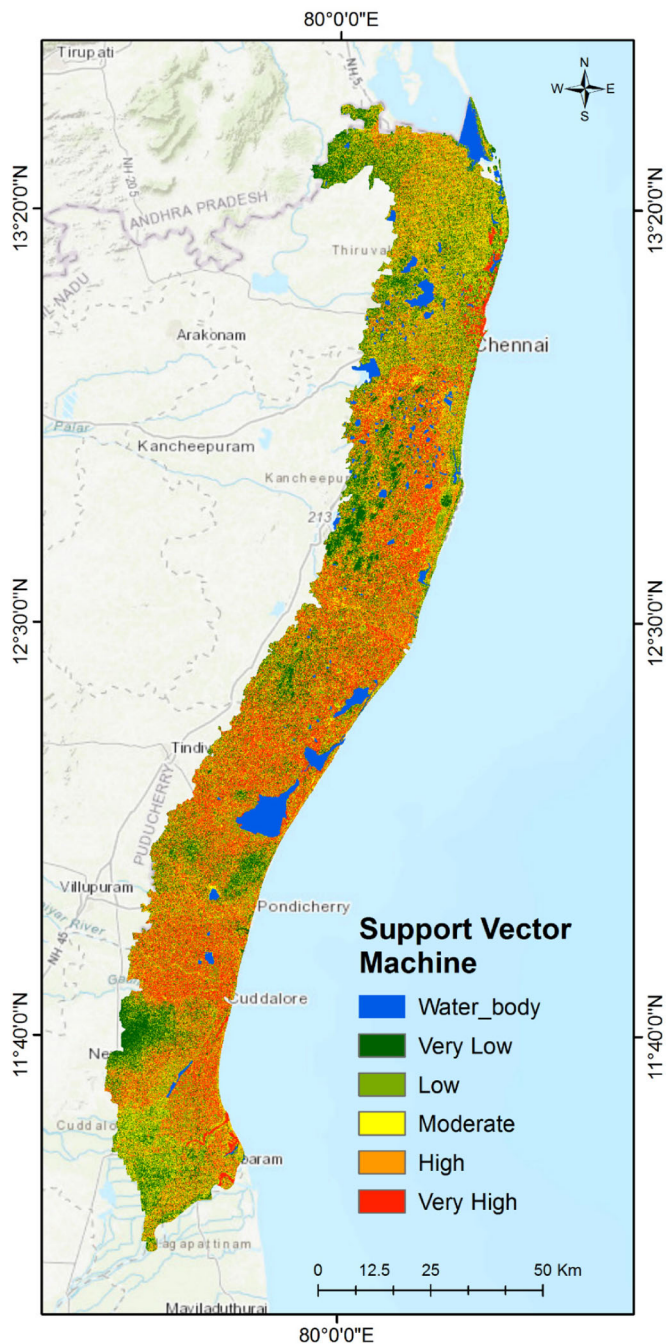


Figure 13. Flood susceptibility map-SVM model.

of 1783.40 sq. km, and the majority area of about 1873.21 sq. km falls into the very high susceptibility zone. From the variable importance (Figure 8) DEM (100) has the highest importance in this model followed by TWI (20.44%), slope (33.53%), ge8-waterbody (27.79%), TRI (32.81%), ge6-deltaic plain (25.61%), g6-coastal sediments (43.89%), ge2-pediment Pedi plain complex (31.20%), ge5-coastal plain (24.42%), STI (15.77%), s1-

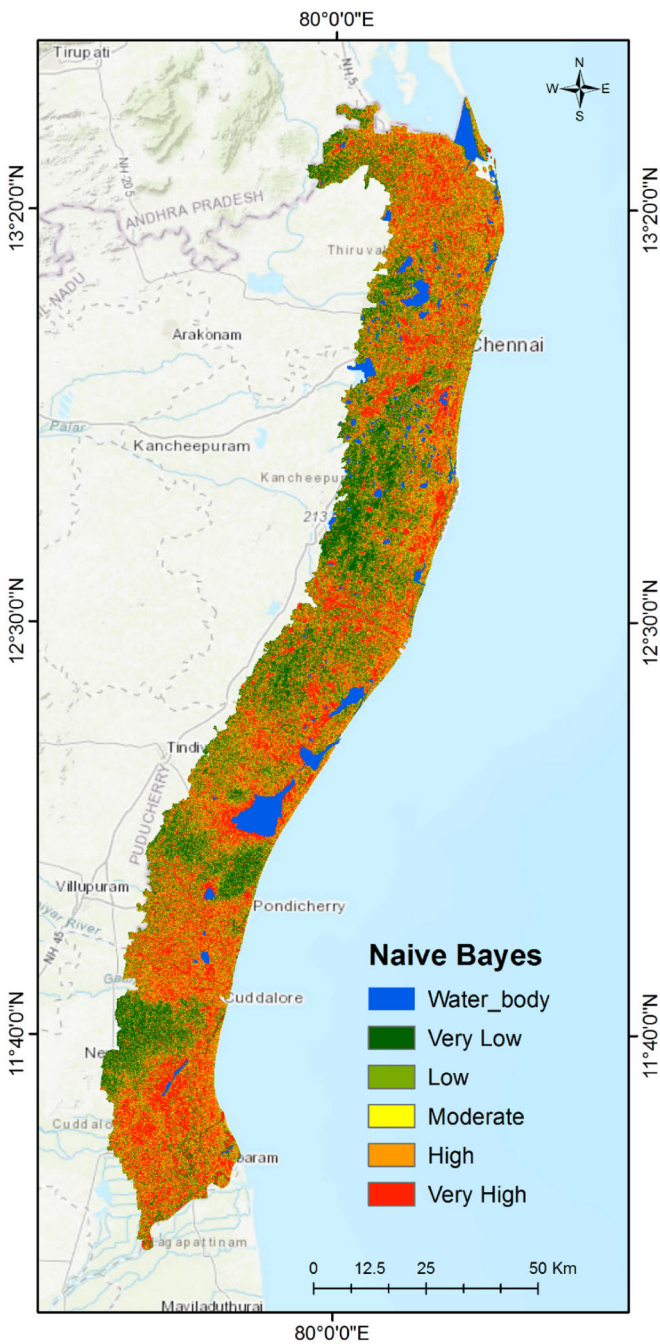


Figure 14. Flood susceptibility map-Naïve Bayes model.

loamy sand (17.93%), whereas NDVI, plan_C, and rainfall are less than 10% of the importance. Tuning parameters fL, adjust and use kernel are held as constant at a value of 0, 1, and True respectively. 'fL' is the Laplace correction which is a smoothing technique that aids in the resolve zero probability problem using higher alpha values. ROC is used to select the optimal model using the largest value. The final values of sigma are

0.05829778 and $C=1$ ([Figure 9E](#)). The accuracy and kappa values being 87% and 72% respectively, and sensitivity and specificity score 95% and 74% for the testing datasets.

4. Discussion

The results of all the five models are evaluated for the effective flood susceptibility mapping of the region. However, the performance of the models is primarily determined by the input data. As a result, it is critical to evaluate and validate the data before using it as an input in learning models. Considering all the 17 parameters, DEM plays an important role as it is the key parameter utilized to create a significant set of input parameters. The slope is an important topographic factor that should be considered in any flood risk assessment. Steep slopes, significantly reducing the absorption amount of the soil, accelerate the surface runoff induced by precipitation. Areas with a low slope are more likely to flood due to excess water stagnation, resulting in severe flooding. As a result, the slope plays a significant role in regulating surface runoff, infiltrations, and water retention, affecting an area's flood susceptibility. The classes (from 0° to 10°) have the highest correlation with flood occurrence. Since the study area is a coastal region, all the other classes are susceptible to flood except high and very high classes. The second important parameter from input data is SPI, which describes the amount of moisture in the soil and the potential of floods to flow downward in the study region. The lower the SPI, the greater the influence of flood occurrence. Lower SPI values are used to specify areas that can accumulate the flow. In this regard, SPI values close to -3.5 have a higher probability of flood occurrence, indicating that the majority of floods in the study area have occurred in locations with lower SPI values. The effect of TWI on floods is examined, and it is observed that areas with high TWI had a substantial influence to flood in the study area. Since the TWI depicts the distribution of moisture in different parts of the soil, when it tends to increase the soil moisture content, flooding increases as well, and it is an important factor influencing flood, and areas with a high (ranging from 15 to 23) values are extremely prone to flooding. A DEM typically provides a large portion of the input factors in susceptibility modelling. As a result, the accuracy of the flood susceptibility is dependent on the quality of the DEM variables utilized in the modelling ([Avand et al. 2022](#)). The lowest class (ranging from 1 m to 15 m) has the highest correlation with flood occurrence. Rainfall is the primary cause of flooding in areas where rain is the only water source. Moreover, the critical amount of rainfall sufficient to induce a flood is determined by several factors and varies spatially. The annual rainfall varies significantly within the study area due to climatic variability. Higher the rainfall, the higher the chance of flood occurrence. The most significant role is played by rainfall exceeding 700 mm in flooding in this study. High rainfall is observed in the northern portion of the study area. Curvature acts as a topographic morphology. Positive curvature indicates that the slope gradient is convex in an upward direction. In contrast, negative curvature implies that the slope gradient is concave in an upward direction, and the slope is flat if the value is zero. The study's plan curvature ranges from -7 to 8 , with the majority of the area falling into the moderate class (-0.2 – 0.3). The TRI denotes the uniform distribution of elevation variation where flooding is more common in areas with low TRI. Low-class values (0.009–0.157) are found in the floodplains and near-shore regions. NDVI reveals the intensity of vegetation cover, but interpretations can be inferred based on the research purpose. Under various situations, NDVI has various impacts on floods. Water flow is reduced and slowed by a higher NDVI value. The vegetation cover allows water to penetrate deeper into the ground, resulting in a reduction in the volume of water and a lower

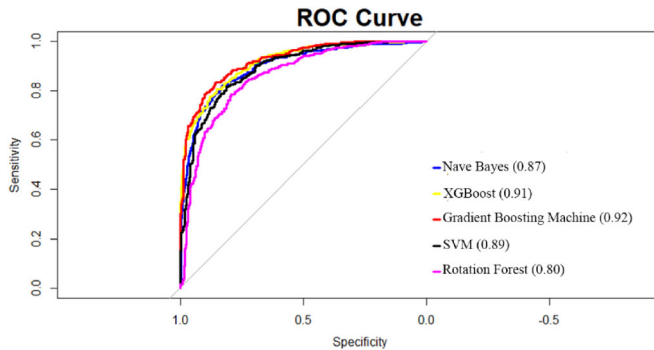


Figure 15. Area under the curves for the models.

chance of a flood event. Low NDVI values ($-0.303\text{--}0.0523$) are typically found in urban areas and along with the river courses. Storms produce higher surge heights with stronger winds; hence wind is one of the critical parameters considered. The northern part of the study area has a band of high wind speed (5.44–6.13) that gradually decreases inwards. The STI depicts the overall runoff plot. Higher runoff areas have higher sediment transport and are less prone to flooding. Areas with low values (0–150) are typically flat, revealing a higher risk of flooding. Geological formations influence the longitudinal profile of streams, causing transient breaks and significantly influencing flood inundation. They also maintain track of the previous flooding, including their intensity and frequency. In this study, the charnockite and coastal sediments class strongly influence floods. The morphology in the study, Pediment plain Complex, and Coastal Plain can substantially impact flood susceptibility. Areas adjacent to active streams are generally more vulnerable to flooding than those further away. The distance from the drainage network has been evaluated to be between 100 and 500 meters for the study.

GBM performs better than all others with an AUC of 92% from the ROC curve (Figure 15). XGBOOST with AUC 91%, rotation forest 80%, SVM 89%, and nave Bayes 87%, Where DEM, slope, TWI, rain, and ge8 are the top five important parameters influencing the high flood. Northern and southern Chennai are especially vulnerable to flooding. On November 8, 2015, the flooding caused extensive damage in Tamil Nadu's northern coastal districts (Chennai's Floods 2021). Northern Chennai's Menjur and Poneri areas and southern Chennai's Velachery, Guindy, and Tambaram are extremely vulnerable to flooding. Tambaram, Kodambakkam, Kundrathur, Chrompet, Selaiyur, Teynampet, Porur, Ashok Nagar, Velachery, and Koyambedu are also frequently affected areas in Chennai. Pondicherry areas are also often flooded, including Harbour, Rainbow Nagar, Krishna Nagar, India Gandhi Statue, Sivaji Statue, and Uzhavar Sandhai. Other blocks in the Cuddalore district such as Kurinjipadi, Panruti, Bhuvanagiri, Keerapalayam, Kattumannarkoil, and Kumaratchi are also frequently flooded. Chennai is the country's second-largest producer of plastic waste, with a daily output of 429 tonnes. During floods, the plastic waste remains to be a great threat clogging the drains and sewers, culminating in the waterlogged streets.

We discussed the factors influencing flood susceptibility and model results, since ML models are robust, they can be effective in evaluating flood susceptibility mapping for other regions when environmental aspects and model input parameters are the same where hydrogeological and topography differences are to be considered. Moreover, the proposed method can be used efficiently to derive flood susceptibility maps for areas with minimal data. Finally, our results can be expanded to susceptibility mapping of other

disasters associated with the flood (water quality, siltation, shoreline change, vegetation loss). Furthermore, the current study will improve understanding of the decision-making process of flood preparedness activities.

5. Conclusion

The research investigated the comparison of different algorithms to improve the individual methods' capability due to the need for an accurate and reliable method to detect flood-prone areas. Five ML algorithms, i.e. GBM, Adaboost, rotation forest, SVM, and NB, are used. From the analysis, the performance of GBM is found to be better than that of the other four models. Seventeen critical parameters are the crucial parameters in the identification of flood susceptibility. According to the study, the major flooding problems are unplanned urbanization and encroachment, ruining existing water bodies, and clogged storm water. Every research has some barriers; consequently, this study had some limitations, such as the lack of hydrological modelling, which even gives more accurate results on flood occurrence concerning time. The important constraint is that we derived the thematic maps using an available 30 m resolution DEM, better resolution of the data will effectively improvise the model results. Accounting the climate change factor and the multiple years of future forecasted LULC into the machine learning models for the flood prediction could be a future scope of the work. The findings of this study can serve as a valuable reference for government bodies in terms of their possible strategic consideration, which might prioritize flood-prone areas.

Authors' contributions

Dr. Subbarayan Saravanan (Conceptualization, Review, and Editing), Devanantham Abijith (Methodology, Data collection and analysis, Writing).

Disclosure statement

The authors declare that there is no conflict of interests regarding the publication of this paper.

ORCID

Subbarayan Saravanan  <http://orcid.org/0000-0003-4085-1195>
Devanantham Abijith  <http://orcid.org/0000-0002-0253-6496>

Data availability statement

The data that supports the findings of this study is available from the corresponding author, upon reasonable request.

References

- Abedi R, Costache R, Shafizadeh-Moghadam H, Pham QB. 2021. Flash-flood susceptibility mapping based on XGBoost, random forest and boosted regression trees. Geocarto Int. 1–18. doi:[10.1080/10106049.2021.1920636](https://doi.org/10.1080/10106049.2021.1920636).
- Abijith D, Saravanan S. 2021. Assessment of land use and land cover change detection and prediction using remote sensing and CA Markov in the northern coastal districts of Tamil Nadu, India. Environ Sci Pollut Res.: 1–13. doi:[10.1007/s11356-021-15782-6](https://doi.org/10.1007/s11356-021-15782-6).

- Abijith D, Saravanan S, Jennifer JJ, Parthasarathy KSS, Singh L, Sankriti R. 2021. Assessing the impact of damage and government response toward the cyclone Gaja in Tamil Nadu, India. *Disaster Resil Sustain.* 577–590. doi:[10.1016/b978-0-323-85195-4.00016-0](https://doi.org/10.1016/b978-0-323-85195-4.00016-0).
- Abraham A, Kundapura S. 2022. Evaluating the long-term trends of the climatic variables over three humid tropical basins in Kerala, India. *Arab J Geosci.* 15(9):1–18.
- Adiat KAN, Nawawi MNM, Abdullah K. 2012. Assessing the accuracy of GIS-based elementary multi criteria decision analysis as a spatial prediction tool – a case of predicting potential zones of sustainable groundwater resources. *J Hydrol.* 440–441:75–89.
- Ahmadolou M, Al-Fugara A, Al-Shabeeb AR, Arora A, Al-Adamat R, Pham QB, Al-Ansari N, Linh NTT, Sajedi H. 2021. Flood susceptibility mapping and assessment using a novel deep learning model combining multilayer perceptron and autoencoder neural networks. *J Flood Risk Manag.* 14(1):e12683.
- Ahmed N, Hoque MA-A, Arabameri A, Pal SC, Chakraborty R, Jui J. 2021. Flood susceptibility mapping in Brahmaputra floodplain of Bangladesh using deep boost, deep learning neural network, and artificial neural network. *Geocarto Int.* 1–22. doi:[10.1080/10106049.2021.2005698](https://doi.org/10.1080/10106049.2021.2005698).
- Akinci H, Zeybek M, Dogan S. 2021. Evaluation of landslide susceptibility of Şavşat district of Artvin Province (Turkey) using machine learning techniques. In: Zhang Y, Cheng Q, editors. *Landslides [working title]*. IntechOpen. doi:[10.5772/intechopen.99864](https://doi.org/10.5772/intechopen.99864).
- Al-Abadi AM. 2018. Mapping flood susceptibility in an arid region of southern Iraq using ensemble machine learning classifiers: a comparative study. *Arab J Geosci.* 11(9):1–19.
- Al-Juaidi AEM, Nassar AM, Al-Juaidi OEM. 2018. Evaluation of flood susceptibility mapping using logistic regression and GIS conditioning factors. *Arab J Geosci.* 11(24):1–10.
- Amarasinghe U, Amarnath G, Alahcoon N, Ghosh S. 2020. How do floods and drought impact economic growth and human development at the sub-national level in India? *Clim.* 8(11):123.
- Arabameri A, Danesh AS, Santosh M, Cerdá A, Pal SC, Ghorbanzadeh O, Roy P, Chowdhuri I. 2022. Flood susceptibility mapping using meta-heuristic algorithms. *Geomat Nat Hazards Risk.* 13(1): 949–974.
- Arabameri A, Saha S, Mukherjee K, Blaschke T, Chen W, Ngo PTT, Band SS. 2020. Modeling spatial flood using novel ensemble artificial intelligence approaches in Northern Iran. *Remote Sens.* 12(20): 3423.
- Avand M, Kuriki A, Khazaei M, Ghorbanzadeh O. 2022. DEM resolution effects on machine learning performance for flood probability mapping. *J Hydro-Environ Res.* 40:1–16.
- Ayyadevara VK. 2018. Gradient boosting machine. *Pro Mach Learn Algorithms.* 117–134. doi:[10.1007/978-1-4842-3564-5_6](https://doi.org/10.1007/978-1-4842-3564-5_6).
- Band SS, Janizadeh S, Pal SC, Saha A, Chakrabortty R, Melesse AM, Mosavi A. 2020a. Flash flood susceptibility modeling using new approaches of hybrid and ensemble tree-based machine learning algorithms. *Remote Sens.* 12(21):3568.
- Band SS, Janizadeh S, Pal SC, Saha A, Chakrabortty R, Melesse AM, Mosavi A. 2020b. Flash flood susceptibility modeling using new approaches of hybrid and ensemble tree-based machine learning algorithms. *Remote Sens.* 12(21):1–23.
- Belousov AI, Verzakov SA, Von Frese J. 2002. Applicational aspects of support vector machines. *J Chemom.* 16(8–10):482–489.
- Bera S, Das A, Mazumder T. 2022. Evaluation of machine learning, information theory and multi-criteria decision analysis methods for flood susceptibility mapping under varying spatial scale of analyses. *Remote Sens Appl Soc Environ.* 25:100686.
- Bilham R, Bali BS. 2014. A ninth century earthquake-induced landslide and flood in the Kashmir Valley, and earthquake damage to Kashmir's Medieval temples. *Bull Earthquake Eng.* 12(1):79–109.
- Boyaj A, Ashok K, Ghosh S, Devanand A, Dandu G. 2018. The Chennai extreme rainfall event in 2015: the Bay of Bengal connection. *Clim Dyn.* 50(7–8):2867–2879.
- Bui DT, Tsangaratos P, Nguyen V-T, Liem NV, Trinh PT. 2020. Comparing the prediction performance of a Deep Learning Neural Network model with conventional machine learning models in landslide susceptibility assessment. *CATENA.* 188:104426.
- Byun H, Lee SW. 2002. Applications of support vector machines for pattern recognition: a survey. *Lect Notes Comput Sci (Including Subser Lect Notes Artif Intell Lect Notes Bioinfo).* 2388:213–236.
- Chakraborty A. 2016. A synoptic-scale perspective of heavy rainfall over Chennai in November 2015. *Curr Sci.* 111(1):201.
- Chakraborty R, Chandra Pal S, Rezaie F, Arabameri A, Lee S, Roy P, Saha A, Chowdhuri I, Moayed H. 2021. Flash-flood hazard susceptibility mapping in Kangsabati River Basin, India. *Geocarto Int.* 1–23. doi:[10.1080/10106049.2021.1953618](https://doi.org/10.1080/10106049.2021.1953618).

- Chen T, Guestrin C. 2016. XGBoost. In Proc 22nd ACM SIGKDD Int Conf Knowl Discov Data Min. New York, NY: ACM. p. 785–794.
- Chen W, Li Y, Xue W, Shahabi H, Li S, Hong H, Wang X, Bian H, Zhang S, Pradhan B, et al. 2020. Modeling flood susceptibility using data-driven approaches of naïve Bayes tree, alternating decision tree, and random forest methods. *Sci Total Environ.* 701:134979.
- Chen W, Pradhan B, Li S, Shahabi H, Rizeei HM, Hou E, Wang S. 2019. Novel hybrid integration approach of bagging-based Fisher's linear discriminant function for groundwater potential analysis. *Nat Resour Res.* 28(4):1239–1258.
- Chowdary VM, Chakraborty D, Jeyaram A, Murthy YVNK, Sharma JR, Dadhwal VK. 2013. Multi-criteria decision making approach for watershed prioritization using analytic hierarchy process technique and GIS. *Water Resour Manage.* 27(10):3555–3571.
- Costache R, Ngo PTT, Bui DT. 2020. Novel ensembles of deep learning neural network and statistical learning for flash-flood susceptibility mapping. *Water.* 12(6):1549.
- Das S. 2019. Geospatial mapping of flood susceptibility and hydro-geomorphic response to the floods in Ulhas basin, India. *Remote Sens Appl Soc Environ.* 14:60–74.
- Falah F, Rahmati O, Rostami M, Ahmadisharaf E, Daliakopoulos IN, Pourghasemi HR. 2019. Artificial neural networks for flood susceptibility mapping in data-scarce urban areas. *Spat Model GIS R Earth Environ Sci.* 323–336. doi:[10.1016/b978-0-12-815226-3.00014-4](https://doi.org/10.1016/b978-0-12-815226-3.00014-4).
- Fan J, Wang X, Wu L, Zhou H, Zhang F, Yu X, Lu X, Xiang Y. 2018. Comparison of Support Vector Machine and Extreme Gradient Boosting for predicting daily global solar radiation using temperature and precipitation in humid subtropical climates: a case study in China. *Energy Convers Manag.* 164: 102–111.
- Fang Z, Wang Y, Duan G, Peng L. 2021. Landslide susceptibility mapping using rotation forest ensemble technique with different decision trees in the Three Gorges Reservoir Area, China. *Remote Sens.* 13(2): 238.
- Friedman JH. 2001. Greedy function approximation: a gradient boosting machine. *Ann Stat.* 29(5): 1189–1232. doi:[10.1214/aos/1013203451](https://doi.org/10.1214/aos/1013203451).
- George SL, Kantamaneni K, V RA, Prasad KA, Shekhar S, Panneer S, Rice L, Balasubramani K. 2022. A multi-data geospatial approach for understanding flood risk in the coastal plains of Tamil Nadu, India. *Earth.* 3(1):383–400.
- Gesch DB. 2018. Best practices for elevation-based assessments of sea-level rise and coastal flooding exposure. *Front Earth Sci.* 6:230.
- Ghimire E, Sharma S, Lamichhane N. 2020. Evaluation of one-dimensional and two-dimensional HEC-RAS models to predict flood travel time and inundation area for flood warning system. *ISH J Hydraul Eng.* 28(1):110–126. doi:[10.1080/0971501020201824621](https://doi.org/10.1080/0971501020201824621).
- Guhathakurta P, Sreejith OP, Menon PA. 2011. Impact of climate change on extreme rainfall events and flood risk in India. *J Earth Syst Sci.* 120(3):359–373.
- Guyon I, Weston J, Barnhill S, Vapnik V. 2002. Gene selection for cancer classification using support vector machines. *Mach Learn.* 46(1/3):389–422.
- Hammami S, Zouhri L, Souissi D, Souei A, Zghibi A, Marzougui A, Dlala M. 2019. Application of the GIS based multi-criteria decision analysis and analytical hierarchy process (AHP) in the flood susceptibility mapping (Tunisia). *Arab J Geosci.* 12(21):1–16.
- He Q, Jiang Z, Wang M, Liu K. 2021. Landslide and wildfire susceptibility assessment in Southeast Asia using ensemble machine learning methods. *Remote Sens.* 13(8):1572.
- Hong H, Liu J, Bui DT, Pradhan B, Acharya TD, Pham BT, Zhu AX, Chen W, Ahmad BB. 2018a. Landslide susceptibility mapping using J48 Decision Tree with AdaBoost, Bagging and Rotation Forest ensembles in the Guangchang area (China). *CATENA.* 163:399–413.
- Hong H, Panahi M, Shirzadi A, Ma T, Liu J, Zhu AX, Chen W, Kougias I, Kazakis N. 2018b. Flood susceptibility assessment in Hengfeng area coupling adaptive neuro-fuzzy inference system with genetic algorithm and differential evolution. *Sci Total Environ.* 621:1124–1141.
- Hong H, Tsangaratos P, Ilia I, Liu J, Zhu AX, Chen W. 2018c. Application of fuzzy weight of evidence and data mining techniques in construction of flood susceptibility map of Poyang County, China. *Sci Total Environ.* 625:575–588.
- IPCC. 2022. AR6 climate change 2022: impacts, adaptation and vulnerability—IPCC. <https://www.ipcc.ch/report/sixth-assessment-report-working-group-ii/>.
- Jacynth Jennifer J, Saravanan S. 2020. Contribution of SAR-driven displacement measurement in assessing the triggering factors of rainfall-induced landslides. *Geocarto Int.* 1–21. doi:[10.1080/10106049.2020.1844313](https://doi.org/10.1080/10106049.2020.1844313).

- Jacinth Jennifer J, Saravanan S, Abijith D. **2022**. Integration of SAR and multi-spectral imagery in flood inundation mapping – a case study on Kerala floods 2018. *ISH J Hydraul Eng.* 28(sup1):480–490.
- Janizadeh S, Chandra Pal S, Saha A, Chowdhuri I, Ahmadi K, Mirzaei S, Mosavi AH, Tiefenbacher JP. **2021**. Mapping the spatial and temporal variability of flood hazard affected by climate and land-use changes in the future. *J Environ Manage.* 298:113551.
- Javidan N, Kavian A, Pourghasemi HR, Conoscenti C, Jafarian Z, Rodrigo-Comino J. **2021**. Evaluation of multi-hazard map produced using MaxEnt machine learning technique. *Sci Rep.* 11(1):1–20.
- Jebrur MN, Pradhan B, Tehrany MS. **2014**. Optimization of landslide conditioning factors using very high-resolution airborne laser scanning (LiDAR) data at catchment scale. *Remote Sens Environ.* 152: 150–165.
- Jennifer JJ, Saravanan S, Pradhan B. **2020**. Persistent Scatterer Interferometry in the post-event monitoring of the Idukki Landslides. *Geocarto Int.* 37(5):1514–1528.
- Jose DM, Vincent AM, Dwarakish GS. **2022**. Improving multiple model ensemble predictions of daily precipitation and temperature through machine learning techniques. *Sci Rep.* 12(1):1–25.
- Joyce J. **2017**. Coupling infrastructure resilience and flood risk assessment for a coastal urban watershed electron. Theses Diss. <https://stars.library.ucf.edu/etd/5573>.
- Ju J, Slingo J. **1995**. The Asian summer monsoon and ENSO. *Q J Royal Met Soc.* 121(525):1133–1168.
- Kalantari Z, Ferreira CSS, Koutsouris AJ, Ahlmer A-K, Cerdà A, Destouni G. **2019**. Assessing flood probability for transportation infrastructure based on catchment characteristics, sediment connectivity and remotely sensed soil moisture. *Sci Total Environ.* 661:393–406.
- Khosravi K, Pham BT, Chapi K, Shirzadi A, Shahabi H, Revhaug I, Prakash I, Tien Bui D. **2018**. A comparative assessment of decision trees algorithms for flash flood susceptibility modeling at Haraz watershed, northern Iran. *Sci Total Environ.* 627:744–755.
- Krishnaraj A, Honnasiddaiah R. **2022**. Remote sensing and machine learning based framework for the assessment of spatio-temporal water quality in the Middle Ganga Basin. *Environ Sci Pollut Res.* 1:1–20.
- Kulithalai Shiyam Sundar P, Deka PC. **2021**. Spatio-temporal classification and prediction of land use and land cover change for the Vembanad Lake system, Kerala: a machine learning approach. *Environ Sci Pollut Res.* 1–17. doi:[10.21203/rs.3.rs-581788/v1](https://doi.org/10.21203/rs.3.rs-581788/v1).
- Lal P, Prakash A, Kumar A, Srivastava PK, Saikia P, Pandey AC, Srivastava P, Khan ML. **2020**. Evaluating the 2018 extreme flood hazard events in Kerala, India. *Remote Sens Lett.* 11(5):436–445.
- Lee S, Kim JC, Jung HS, Lee MJ, Lee S. **2017**. Spatial prediction of flood susceptibility using random-forest and boosted-tree models in Seoul metropolitan city, Korea. *Geomat Nat Hazards Risk.* 8(2): 1185–1203.
- Lee S, Lee M-J, Jung H-S, Lee S. **2020**. Landslide susceptibility mapping using Naïve Bayes and Bayesian network models in Umyeonsan, Korea. *Geocarto Int.* 35(15):1665–1679.
- Lindsay JB, Newman DR, Francioni A. **2019**. Scale-optimized surface roughness for topographic analysis. *Geosci.* 9(7):322.
- Madhuri R, Sistla S, Srinivasa Raju K. **2021**. Application of machine learning algorithms for flood susceptibility assessment and risk management. *J Water Clim Chang.* 12(6):2608–2623.
- Minh HVT, Avtar R, Mohan G, Misra P, Kurasaki M. **2019**. Monitoring and mapping of rice cropping pattern in flooding area in the Vietnamese Mekong delta using Sentinel-1A data: a case of an Giang province. *ISPRS Int J Geo-Inform.* 8(5):211. doi:[10.3390/ijgi8050211](https://doi.org/10.3390/ijgi8050211).
- Mohammadi A, Kamran KV, Karimzadeh S, Shahabi H, Al-Ansari N. **2020**. Flood detection and susceptibility mapping using sentinel-1 time series, alternating decision trees, and bag-ADTree Models. *Complexity.* 2020:1–21.
- Moore ID, Grayson RB, Ladson AR. **1991**. Digital terrain modelling: a review of hydrological, geomorphological, and biological applications. *Hydrolog Process.* 5(1):3–30.
- Mudashiru RB, Sabtu N, Abustan I. **2021**. Quantitative and semi-quantitative methods in flood hazard/susceptibility mapping: a review. *Arab J Geosci.* 14(11):1–24.
- Naghibi SA, Dolatkordestani M, Rezaei A, Amouzegari P, Heravi MT, Kalantar B, Pradhan B. **2019**. Application of rotation forest with decision trees as base classifier and a novel ensemble model in spatial modeling of groundwater potential. *Environ Monit Assess.* 191(4):1–20.
- Narasimhan B, Madras I, Murty Bhallamudi S, Mondal A, Bombay I, Ghosh S, Mujumdar P, Bangalore I, Mujumdar P. **2016**. Chennai floods 2015 a rapid assessment [Internet]. <http://www.icwar.iisc.ac.in/wp-content/uploads/2016/06/Chennai-Floods-Rapid-Assessment-Report.pdf>.
- Parida Y. **2020**. Economic impact of floods in the Indian states. *Environ Dev Econ.* 25(3):267–290.
- Parthasarathy KSS, Deka PC. **2019**. Remote sensing and GIS application in assessment of coastal vulnerability and shoreline changes: a review. *ISH J Hydraul Eng.* 27(sup1):588–600.

- Parthasarathy KSS, Deka PC, Saravanan S, Abijith D, Jacinth Jennifer J. **2021**. Assessing the impact of 2018 tropical rainfall and the consecutive flood-related damages for the state of Kerala, India. *Disaster Resil Sustain.* 379–395. doi:[10.1016/b978-0-323-85195-4.00013-5](https://doi.org/10.1016/b978-0-323-85195-4.00013-5).
- Parthasarathy KSS, Saravanan S, Deka PC, Devanantham A. **2022**. Assessment of potentially vulnerable zones using geospatial approach along the coast of Cuddalore district, East coast of India. *ISH J Hydraul Eng.* 28(sup1):422–432.
- Pham BT, Phong TV, Nguyen HD, Qi C, Al-Ansari N, Amini A, Ho LS, Tuyen TT, Yen HPH, Ly H-B, et al. **2020**. A comparative study of kernel logistic regression, radial basis function classifier, multinomial Naive Bayes, and logistic model tree for flash flood susceptibility mapping. *Water (Switzerland).* 12(1):239.
- Pham BT, Prakash I. **2017**. Evaluation and comparison of LogitBoost Ensemble, Fisher's Linear Discriminant Analysis, logistic regression and support vector machines methods for landslide susceptibility mapping. *Geocarto Int.* 34(3):316–333. doi:[10.1080/1010604920171404141](https://doi.org/10.1080/1010604920171404141).
- Pham QB, Pal SC, Chakrabortty R, Norouzi A, Golshan M, Ogunrinde AT, Janizadeh S, Khedher KM, Anh DT. **2021**. Evaluation of various boosting ensemble algorithms for predicting flood hazard susceptibility areas. *Geomat Nat Hazards Risk.* 12(1):2607–2628.
- Pouyan S, Pourghasemi HR, Bordbar M, Rahmanian S, Clague JJ. **2021**. A multi-hazard map-based flooding, gully erosion, forest fires, and earthquakes in Iran. *Sci Rep.* 11(1):1–19.
- Pradhan B. **2013**. A comparative study on the predictive ability of the decision tree, support vector machine and neuro-fuzzy models in landslide susceptibility mapping using GIS. *Comput Geosci.* 51: 350–365.
- Rahman M, Chen N, Elbeltagi A, Islam MM, Alam M, Pourghasemi HR, Tao W, Zhang J, Shufeng T, Faiz H, et al. **2021a**. Application of stacking hybrid machine learning algorithms in delineating multi-type flooding in Bangladesh. *J Environ Manage.* 295:113086.
- Rahman M, Chen N, Islam MM, Mahmud GI, Pourghasemi HR, Alam M, Rahim MA, Baig MA, Bhattacharjee A, Dewan A. **2021b**. Development of flood hazard map and emergency relief operation system using hydrodynamic modeling and machine learning algorithm. *J Clean Prod.* 311:127594.
- Rahman M, Ninghseng C, Mahmud GI, Islam MM, Pourghasemi HR, Ahmad H, Habumugisha JM, Washakh RMA, Alam M, Liu E, et al. **2021c**. Flooding and its relationship with land cover change, population growth, and road density. *Geosci Front.* 12(6):101224.
- Rahmati O, Kalantari Z, Samadi M, Uuemaa E, Moghaddam DD, Nalivan OA, Destouni G, Bui DT. **2019**. GIS-based site selection for check dams in watersheds: considering geomorphometric and topohydrological factors. *Sustain.* 11(20):5639.
- Rodríguez JJ, Kuncheva LI, Alonso CJ. **2006**. Rotation forest: a new classifier ensemble method. *IEEE Trans Pattern Anal Mach Intell.* 28(10):1619–1630.
- Sachdeva S, Bhatia T, Verma AK. **2017**. Flood susceptibility mapping using GIS-based support vector machine and particle swarm optimization: a case study in Uttarakhand (India). *8th Int Conf Comput Commun Netw Technol ICCNT 2017.*
- Sachdeva S, Kumar B. **2022**. Flood susceptibility mapping using extremely randomized trees for Assam 2020 floods. *Ecol Inform.* 67:101498.
- Sagarika S, Kalra A, Ahmad S. **2016**. Pacific Ocean SST and Z500 climate variability and western U.S. seasonal streamflow. *Int J Climatol.* 36(3):1515–1533.
- Saha A, Pal SC, Arabameri A, Blaschke T, Panahi S, Chowdhuri I, Chakrabortty R, Costache R, Arora A. **2021**. Flood susceptibility assessment using novel ensemble of hyperpipes and support vector regression algorithms. *Water (Switzerland).* 13(2):241.
- Sahin EK. **2020**. Assessing the predictive capability of ensemble tree methods for landslide susceptibility mapping using XGBoost, gradient boosting machine, and random forest. *SN Appl Sci.* 2(7):1–17.
- Saleem Khan A, Sabuj Kumar M, Sudhir Chella R, Devdyuti B. **2020**. Chennai city and coastal hazards: addressing community-based adaptation through the lens of climate change and sea-level rise (CBACCS). *Clim Chang Manag.* 777–798. doi:[10.1007/978-3-030-37425-9_39](https://doi.org/10.1007/978-3-030-37425-9_39).
- Saleh A, Yuzir A, Sabtu N. **2022**. Flash flood susceptibility mapping of Sungai Pinang catchment using frequency ratio. *JSM.* 51(1):51–65.
- Samanta S, Pal DK, Palsamanta B. **2018**. Flood susceptibility analysis through remote sensing, GIS and frequency ratio model. *Appl Water Sci.* 8(2):1–14.
- Samui P. **2008**. Slope stability analysis: a support vector machine approach. *Environ Geol.* 56(2):255–267.
- Sanyal J, Lu XX. **2004**. Application of remote sensing in flood management with special reference to monsoon Asia: a review. *Nat Hazards.* 33(2):283–301.

- Saranya T, Saravanan S. 2021. Evolution of a hybrid approach for groundwater vulnerability assessment using hierarchical fuzzy-DRASTIC models in the Cuddalore Region, India. Environ Earth Sci. 80(5). doi:[10.1007/s12665-021-09479-9](https://doi.org/10.1007/s12665-021-09479-9).
- Saranya T, Saravanan S. 2022. Assessment of groundwater vulnerability using analytical hierarchy process and evidential belief function with DRASTIC parameters, Cuddalore, India. Int J Environ Sci Technol. 1-20. doi:[10.1007/s13762-022-03944-z](https://doi.org/10.1007/s13762-022-03944-z).
- Saravanan S, Jennifer J, Singh L, D A. 2018. Cyclone vulnerability assessment of Cuddalore coast in Tamil Nadu, India using remote sensing, and GIS. In: Haigh R, Comfort L, Hakam A, Ismail FA, editors. MATEC Web Conf. Vol. 229:02022.
- Saravanan S, Parthasarathy KSS, Sivarajanji S. 2019a. Assessing coastal aquifer to seawater intrusion: application of the GALDIT method to the Cuddalore Aquifer, India. Coast Zo Manag Glob Perspect Reg Process Local Issues. 233-250. doi:[10.1016/b978-0-12-814350-6.00010-0](https://doi.org/10.1016/b978-0-12-814350-6.00010-0).
- Saravanan S, Parthasarathy KSS, Vishnuprasath SR. 2019b. Monitoring spatial and temporal scales of shoreline changes in the Cuddalore Region, India. Coast Zo Manag Glob Perspect Reg Process Local Issues. 99-112. doi:[10.1016/b978-0-12-814350-6.00004-5](https://doi.org/10.1016/b978-0-12-814350-6.00004-5).
- Sarkar D, Mondal P. 2019. Flood vulnerability mapping using frequency ratio (FR) model: a case study on Kulik river basin, Indo-Bangladesh Barind region. Appl Water Sci. 10(1):1-13.
- Schumann GJP, Moller DK. 2015. Microwave remote sensing of flood inundation. Phys Chem Earth, Parts A/B/C. 83-84:84-95.
- Shahabi H, Shirzadi A, Ronoud S, Asadi S, Pham BT, Mansouripour F, Geertsema M, Clague JJ, Bui DT. 2021. Flash flood susceptibility mapping using a novel deep learning model based on deep belief network, back propagation and genetic algorithm. Geosci Front. 12(3):101100.
- Shen Y, Morsy MM, Huxley C, Tahvildari N, Goodall JL. 2019. Flood risk assessment and increased resilience for coastal urban watersheds under the combined impact of storm tide and heavy rainfall. J Hydrol. 579:124159.
- Singh L, Saravanan S. 2020. Impact of climate change on hydrology components using CORDEX South Asia climate model in Wunna, Bharathpuzha, and Mahanadi, India. Environ Monit Assess. 192(11): 1-21.
- Swain KC, Singha C, Nayak L. 2020. Flood susceptibility mapping through the GIS-AHP technique using the cloud. IJGI. 9(12):720.
- Tamaddun KA, Kalra A, Bernardez M, Ahmad S. 2019. Effects of ENSO on temperature, precipitation, and potential evapotranspiration of North India's monsoon: an analysis of trend and entropy. Water. 11(2):189.
- Tehrany MS, Jones S, Shabani F. 2019. Identifying the essential flood conditioning factors for flood prone area mapping using machine learning techniques. CATENA. 175:174-192.
- Tehrany MS, Kumar L. 2018. The application of a Dempster-Shafer-based evidential belief function in flood susceptibility mapping and comparison with frequency ratio and logistic regression methods. Environ Earth Sci. 77(13):1-24.
- Tehrany MS, Pradhan B, Jebur MN. 2015. Flood susceptibility analysis and its verification using a novel ensemble support vector machine and frequency ratio method. Stoch Environ Res Risk Assess. 29(4): 1149-1165.
- Tehrany MS, Pradhan B, Jebur MN, Tehrany MS, Pradhan B, Jebur MN. 2013. Spatial prediction of flood susceptible areas using rule based decision tree (DT) and a novel ensemble bivariate and multivariate statistical models in GIS. J Hydrol. 504:69-79.
- Tien Bui D, Hoang ND, Pham TD, Ngo PTT, Hoa PV, Minh NQ, Tran XT, Samui P. 2019a. A new intelligence approach based on GIS-based Multivariate Adaptive Regression Splines and metaheuristic optimization for predicting flash flood susceptible areas at high-frequency tropical typhoon area. J Hydrol. 575:314-326.
- Tien Bui D, Shirzadi A, Chapi K, Shahabi H, Pradhan B, Pham BT, Singh VP, Chen W, Khosravi K, Bin Ahmad B, et al. 2019b. A hybrid computational intelligence approach to groundwater spring potential mapping. Water (Switzerland). 11(10):2013-2030.
- Towfiqul Islam ARM, Talukdar S, Mahato S, Kundu S, Eibek KU, Pham QB, Kuriqi A, Linh NTT. 2021. Flood susceptibility modelling using advanced ensemble machine learning models. Geosci Front. 12(3): 101075.
- Vafakhah M, Mohammad Hasani Loor S, Pourghasemi H, Katebikord A. 2020. Comparing performance of random forest and adaptive neuro-fuzzy inference system data mining models for flood susceptibility mapping. Arab J Geosci. 13(11):1-16.
- Vaze J, Teng J, Spencer G. 2010. Impact of DEM accuracy and resolution on topographic indices. Environ Model Softw. 25(10):1086-1098.

- Vojtek M, Vojteková J, Costache R, Pham QB, Lee S, Arshad A, Sahoo S, Linh NTT, Anh DT. **2021**. Comparison of multi-criteria-analytical hierarchy process and machine learning-boosted tree models for regional flood susceptibility mapping: a case study from Slovakia. *Geomat Nat Hazards Risk*. 12(1): 1153–1180.
- Walczkiewicz T, Skonieczna M. **2020**. Rainfall flooding in urban areas in the context of geomorphological aspects. *Geosciences*. 10(11):457.
- Wang Y, Colby JD, Mulcahy KA. **2010**. An efficient method for mapping flood extent in a coastal floodplain using Landsat TM and DEM data. *Int J Remote Sens*. 23(18):3681–3696. doi:[10.1080/01431160110114484](https://doi.org/10.1080/01431160110114484).
- Wang Z, Lai C, Chen X, Yang B, Zhao S, Bai X. **2015**. Flood hazard risk assessment model based on random forest. *J Hydrol*. 527:1130–1141.
- Ward PJ, Jongman B, Kummu M, Dettinger MD, Weiland FCS, Winsemius HC. **2014**. Strong influence of El Niño Southern Oscillation on flood risk around the world. *Proc Natl Acad Sci U S A*. 111(44): 15659–15664.
- Yan J, Jin J, Chen F, Yu G, Yin H, Wang W. **2018**. Urban flash flood forecast using support vector machine and numerical simulation. *J Hydroinfo*. 20(1):232–245.
- Zzaman RU, Nowreen S, Billah M, Islam AS. **2021**. Flood hazard mapping of Sangu River basin in Bangladesh using multi-criteria analysis of hydro-geomorphological factors. *J Flood Risk Manag*. 14(3). doi:[10.1111/jfr3.12715](https://doi.org/10.1111/jfr3.12715).